Solar-Terrestrial Physics. 2026, vol. 12, iss.1, pp. 68–86. DOI: 10.12737/stp-121202609. © 2026 M.A. Chernigovskaya, D.S. Khabituev, A.G. Setov, K.G. Ratovsky, A.S. Kalishin, S.A. Dolgacheva, A.E. Stepanov, A.Yu. Belinskaya, V.V. Bychkov, S.A. Grigorieva, V.A. Panchenko, A.V. Timchenko. Published by INFRA-M Academic Publishing House

DOI: 10.12737/stp-121202609
EDN: FRFUOG

Received July 08, 2025
Accepted October 06, 2025

THERMOSPHERIC EFFECTS DURING THE MAGNETIC SUPERSTORMS IN MAY 2024 AND OCTOBER–NOVEMBER 2003 IN THE NORTHERN HEMISPHERE AND THE IONOSPHERIC RESPONSE TO THEM

M.A. Chernigovskaya
Institute of Solar-Terrestrial Physics SB RAS, Irkutsk, Russia, cher@iszf.irk.ru

D.S. Khabituev
Institute of Solar-Terrestrial Physics SB RAS, Irkutsk, Russia, Khabituev@iszf.irk.ru

A.G. Setov
Institute of Solar-Terrestrial Physics SB RAS, Irkutsk, Russia, setov@iszf.irk.ru

K.G. Ratovsky
Institute of Solar-Terrestrial Physics SB RAS, Irkutsk, Russia, ratovsky@iszf.irk.ru

A.S. Kalishin
Arctic and Antarctic Research Institute, Saint Petersburg, Russia, askalishin@aari.ru

S.A. Dolgacheva
Arctic and Antarctic Research Institute, Saint Petersburg, Russia, dolgacheva@aari.ru

A.E. Stepanov
Yu.G. Shafer Institute of Cosmophysical Research and Aeronomy SB RAS, Yakutsk, Russia, a_e_stepanov@ikfia.sbras.ru

A.Yu. Belinskaya
Trofimuk Institute of Petroleum Geology and Geophysics SB RAS, Novosibirsk, Russia, belinskayaay@ipgg.sbras.ru

V.V. Bychkov
Institute of Cosmophysical Research and Radio Wave Propagation FEB RAS, Paratunka, Russia, vasily.v.bychkov@gmail.com

S.A. Grigorieva
Institute of Geophysics UB RAS, Ekaterinburg, Russia, ion@arti.igfuroran.ru

V.A. Panchenko
Pushkov Institute of Terrestrial Magnetism, Ionosphere, and Radio Wave Propagation RAS, Moscow, Troitsk, Russia, panch@izmiran.ru

A.V. Timchenko
West Department of Pushkov Institute of Terrestrial Magnetism, Ionosphere and Radio Wave Propagation RAS, Kaliningrad, Russia, timchenko.leks@gmail.com

Abstract. We study the spatiotemporal variations of ionospheric parameters over the regions of Eurasia by analyzing data from chains of high- and mid-latitude ionosondes during the extreme magnetic storm in May 2024. The analysis of ionospheric parameters allowed us to note strong latitudinal and longitudinal differences in variations of the analyzed parameters under quiet conditions before the onset of the magnetic storm and during its development. Almost immediately after the onset of the storm at 17:00 UT on May 10, 2024, according to data from all ionosondes, a sharp drop in the electron density at the height of the F2-layer maximum was recorded, regardless of the local time at the measurement point. Ionosondes of the high-latitude chain showed a complete absence of data (radio signal blackout) during the main and early recovery phases of the storm until the evening of May 12, 2024, i.e. more than one and a half days. Additional bursts of geomagnetic activity during the recovery phase of the storm were also accompanied by significant and prolonged decreases in the electron density according to ionosonde measurements at all longitudes of Eurasia. The recovery of ionospheric ionization began on May 14–15 at all longitudes of the mid- and high-latitude regions of Eurasia. A long-term negative disturbance of electron density covering a huge territory of mid-latitude Eurasia was caused by an extraordinary, catastrophic drop in the $[O]/[N_2]$ ratio according to satellite measurements of GUVI TIMED during the superstorm for almost three days. The response of the thermospheric composition of neutral gas to the processes developing at high latitudes of the Northern Hemisphere on May 10–15, 2024 was global, with penetration of the thermospheric disturbance at almost all longitudes up to the equatorial latitudes (~10° N) and with very low values of the $[O]/[N_2]$ ratio ~0.1÷0.4. Significant differences in the spatiotemporal variations of the thermospheric composition of neutral gas were revealed during the most extreme geomagnetic storms of the current 21st century — in May 2024 and October–November 2003 (Halloween storms). The magnetic superstorm in May 2024 was much more geoeffective than the superstorms in October–November 2003, and caused a significantly different ionospheric response at different longitudes and latitudes of the Northern Hemisphere.

Keywords: mid- and high-latitude ionosphere, ionosonde chains, geomagnetic storm, variations of ionospheric parameters.

INTRODUCTION

The paper reports the results of a study of thermospheric and ionospheric effects caused by the strongest (*Dst*=–406 nT) geomagnetic disturbance of solar activity cycle 25 on May 10–11, 2024. Following the initiative of colleagues [Chernyshov et al., 2025], we will call this outstanding event in solar-terrestrial physics the Victory Day 2024 geomagnetic storm, since solar flares that led to significant disturbances of Earth's ionosphere occurred on May 8–9, 2024. It is a common practice to name such extreme geomagnetic storms after the days when, for example, solar flares, coronal mass ejections took place, or a maximum effect in the ionosphere was observed (such as the Halloween 2003 storm, St. Patrick's Day 2015 geomagnetic storm, etc.). «Victory Day is a holiday that celebrates the victory of the Soviet Union over Nazi Germany on May 8 (May 9 Moscow time) in 1945. Many countries also celebrated this day as Victory Day or Europe Day on May 8 or 9. After huge human losses during the World War II, Victory Day became an occasion for worldwide celebration» [Chernyshov et al., 2025].

In the entire history of observations, the strongest magnetic storm occurred on September 2, 1859 (Carrington Event) with estimated *Dst* values from –850 to –1760 nT. The most intense geomagnetic storm of the past century was observed on May 13–15, 1921 (estimated *Dst*=–907±132 nT). Such low *Dst* values make these two events the strongest on record.

Since the beginning of the calculation of the *Dst* index in 1957 [Sugiura, Kamei, 1991], the severest geomagnetic disturbance was on March 13, 1989 (Quebec Event) with minimum *Dst*=–589 nT. From 1957 to the end of the 20th century, only three magnetic storms (September 13, 1957, February 11, 1958, July 15–16, 1959) had comparable minimum *Dst* values. The February 11, 1958 geomagnetic storm, which was accompanied by the famous planetary mid-latitude aurora, showed minimum *Dst*=–426 nT.

The strongest magnetic storms in the first two decades of the 21st century happened in the fall of 2003: on October 29–31 (*Dst*=–401 nT) (Halloween storm) and November 20 (*Dst*=–472 nT), and related to G5-level superstorms [Gopalswamy et al., 2005].

Thus, the magnetic storm in May 2024 ranks among the strongest magnetic storms on record. The geomagnetic event of such high intensity has undoubtedly aroused great interest among researchers of atmospheric-ionospheric-magnetospheric coupling. The expected consequences of the impact of the severest magnetic disturbance on Earth might have been problems with the reliability of radio and mobile communications, navigation and location (deterioration of GPS and high-frequency communications can lead to disorientation of vehicles — ships, airplanes, etc.), as well as with power systems. The geomagnetic storm's impact zone covers pipelines, railways, and power transmission lines. Fluxes of high-energy solar wind particles and radiation have a deleterious effect on multipurpose satellite equipment, including life support systems for astronauts during a heliogeomagnetic disturbance. A recent example is the situation with the moderate G2-class magnetic storm on February 2–3, 2022, after which 40 of 49 Starlink satellites, launched a few days earlier, were actually disabled [Berger et al., 2023].

The first and most obvious manifestation of the impact of the magnetic disturbance on Earth was the almost ubiquitous cases of visual observation of aurora during this event. These observations, carried out both with scientific optical instruments and with ordinary smartphones and cameras by millions of people, proved invaluable for obtaining data on this exceptional natural event. Moreover, the fact that the event occurred near the summer solstice in the Northern Hemisphere meant that many optical instruments did not work due to the lack of suitable unlit (dark) conditions [Grandin et al., 2024; Hayakawa et al., 2025]. Consolidated reports by almost seven hundred citizen scientists from more than 30 countries have been compiled. Based on the analysis of the collected data, it was concluded that the aurora was mainly seen in regions with geomagnetic latitudes ranging from 60° to 30° N, and in some cases at lower latitudes. This was much closer to the equator than predicted by auroral oval models, such as the OVATION Prime model [Newell et al., 2014; Grandin et al., 2024].

Such a strong expansion of the auroral region to the equator indirectly indicated an equally strong equatorward shift of the subauroral ionosphere region adjacent to the auroral oval from lower latitudes. A characteristic large-scale spatial structural feature of the subauroral ionosphere is the main ionospheric trough (MIT) of ionization. The MIT minimum is located no more than 5° equatorially from the auroral oval boundary [Rodger et al., 1992; Aladjev et al., 2001; Karpachev, 2003; Deminov, Shubin, 2018; Karpachev, 2021].

In addition to the practical interest sparked by the influence of the most intense geomagnetic disturbances on human living conditions and health, events of this class are of great interest from a scientific point of view. During magnetic storms, a whole complex of intricate processes develops in the ionosphere (ionospheric storms, negative and positive), as a result of which its parameters change significantly [Matsushita, 1959; Prölss, 1995; Rishbeth, 1998; Buonsanto, 1999; Mikhailov, 2000]. The cause of disturbances in Earth's ionosphere is primarily a sequence of interrelated events that begins with manifestations of increased solar activity, which then affect the solar wind—magnetosphere—ionosphere system. In other cases, ionospheric disturbances may be triggered by internal factors of the ionosphere—thermosphere system, which are associated with processes in the neutral atmosphere. In both cases, ionospheric ionization disturbances of varying intensity occur which give rise to ionospheric irregularities of different spatial and time scales. The development of negative and positive effects of ionospheric storms strongly depends on the local time, season, and geographic region [Prölss, 1995; Rishbeth, 1998; Buonsanto, 1999; Mendillo, 2006; Burešová et al., 2007; Ratovsky et al., 2020].

Precipitation of high-energy charged particles from the magnetosphere into the ionosphere, intense electric fields and currents are among the main mechanisms for the formation of various structural features and irregularities in the large-scale structure of the high-latitude ionosphere during periods of increased geomagnetic activity. An increase in currents in a westerly direction in the high-latitude region during magnetic storms induces the motion of neutral gas at thermospheric heights (winds), which redistribute the neutral composition of the atmosphere over most of the high-latitude region and part of the mid-latitude region. Processes in the neutral atmosphere form an integral part of the complex sequence of electrodynamic and chemical processes developing in the ionosphere—thermosphere system during periods of heliogeomagnetic activity. Above the turbopause (~120 km), diffusion separation of atmospheric gases begins. The higher the temperature, the more oxygen is in the atomic state. At altitudes 200–300 km and higher, atomic oxygen becomes predominant, which, as a lighter gas, is transferred faster than molecular nitrogen. This, in turn, leads to a decrease in $[O]/[N_2]$ in the upper atmosphere and hence to negative disturbances of the electron density in the F-region of the ionosphere [Danilov, 2003; Laštovička, 2002; Liou et al., 2005; Prölss, Werner, 2002].

In [Chernigovskaya et al., 2021; Chernigovskaya et al., 2023, 2024a, b], comprehensive studies were carried out of spatiotemporal variations in geomagnetic, ionospheric, and atmospheric parameters at middle and high latitudes of the Northern Hemisphere during extreme magnetic storms in March and June 2015 and a series of magnetic storms in March 2012 and October 2016. The analysis was based on vertical sounding data on ionospheric electron density, obtained by ionosondes of Eurasian high- and mid-latitude chains; total electron content (TEC) data from measurements made by chains of high- and mid-latitude dual-frequency phase GPS/GLONASS receivers, as well as satellite data on $[O]/[N_2]$ in the thermospheric gas column above 100 km from the ultraviolet (UV) spectrometer GUVI (Global Ultraviolet Imager) TIMED (Thermosphere Ionosphere Mesosphere Energetics and Dynamics). Joint analysis of data from ground and satellite radiophysical and spectrometric measurements has yielded very interesting results indicating the presence of significant longitude and latitude differences in ionospheric parameters associated with the formation of vast regions of thermospheric gas with decreased $[O]/[N_2]$. These disturbed active regions of neutral gas, covering not only high but also middle latitudes, are formed in the lower thermosphere of polar latitudes in the night sector during strong westward electrojet in the magnetic storm main phase and have a wave-like spatial structure. Due to the high frequency of molecular ion-neutral collisions, such a wave acquires a large scale and momentum and travels in a westerly direction over long distances. After the magnetic storm ends and the magnetospheric source is "switched off", disturbances at auroral latitudes of the thermospheric gas region with decreased $[O]/[N_2]$ continue to move westward by inertia for several more days, causing electron density variations along the propagation path. Thus, the ionospheric storm effect may last for several more days after the end of the magnetic storm, since the neutral gas composition disturbances, triggered during the development of the magnetic storm and resulting in ionospheric electron density variations, still persist.

In this paper, we continue our research and perform a comprehensive analysis of spatiotemporal features of ionospheric irregularities over Eurasia, using previously developed methods based on ionosonde measurements for the extraordinarily intense magnetic storm in May 2024. Of particular interest and topicality is the comparative analysis, conducted in this study, of the response of the neutral thermospheric gas composition to the most intense geomagnetic disturbances of the 21st century, as well as ionospheric effects observed in the electron density during the superstorms of 2024 and 2003.

EXPERIMENTAL DATA IN USE

To analyze the spatiotemporal variations in ionospheric parameters during the extreme geomagnetic disturbance in May 2024, we employ data on hourly average (or hourly for ionosondes in Novosibirsk and Kaliningrad) values of the F2-layer critical frequency f_oF2 from mid- and high-latitude ionosonde chains. The high-latitude chain consists of six ionosondes located in the latitude range 67–71° N (geomagnetic latitudes 58°<GMlat<64° N) in the longitude sector 26–129° E in Eurasia (Figure 1, red marks; Table 1). The chain includes ionosondes from Russian scientific organizations: DPS-4 (ISTP SB RAS, SHICRA SB RAS) in the stations Norilsk, Zhigansk [Reinisch et al., 1997] and CADI (AARI, Roshydromet) in the stations Lovozero, Salekhard, Tixie Bay [MacDougall et al., 1995; Vystavnoi et al., 2013; Kalishin et al., 2020]. We also use data from the SO166 (Alpha Wolf) ionosonde [Enell et al., 2016] installed in Sodankylä Geophysical Observatory (Finland).

The mid-latitude chain comprises eight ionosondes in the latitude range 52–62° N (42° N<GMlat<54° N)

Figure 1. Map of high-latitude (red marks) and mid-latitude (white marks) ionosonde chains

Table 1

Ionosondes of the high-latitude chain

Ionosonde	Ionosonde	Geographic coordinates		Geomagnetic coordinates	
		latitude	longitude	latitude	longitude
Sodankylä	SO166	67° N	26° E	64° N	118° E
Lovozero	CADI	68° N	35° E	64° N	126° E
Salekhard	CADI	67° N	67° E	59° N	150° E
Norilsk	DPS-4	69° N	88° E	60° N	166° E
Zhigansk	DPS-4	67° N	123° E	58° N	168° W
Tixie Bay	CADI	71°N	129° E	63° N	165° W

Table 2

Ionosondes of the mid-latitude chain

Ionosonde	Ionosonde	Geographic coordinates		Geomagnetic coordinates	
		latitude	longitude	latitude	longitude
Juliusruh	DPS-4D	55° N	13° E	54° N	99° E
Kaliningrad	Parus-A	55° N	21° E	53° N	106° E
Moscow	DPS-4	56° N	37° E	52° N	122° E
Ekaterinburg	Parus-3.0	57° N	60° E	50° N	141° E
Novosibirsk	Ionosonde-MS	55° N	83° E	50° N	160° E
Irkutsk	DPS-4	52° N	104° E	42° N	177° E
Yakutsk	DPS-4	62° N	130° E	53° N	163° W
Paratunka	Parus-2.0	53° N	158° E	46° N	138° W

in the longitude sector 13–158° E (see Figure 1, white marks and captions; Table 2): four digital ionosondes DPS-4 of various modifications (SHICRA SB RAS, Yakutsk; ISTP SB RAS, Irkutsk; IZMIRAN, Moscow; Institute of Atmospheric Physics, Juliusruh, Germany) [Reinisch et al., 1997], three Parus ionosondes of various modifications (IKIR FEB RAS, Paratunka; IGP UrB RAS, Ekaterinburg; WD IZMIRAN, Kaliningrad) [Krasheninnikov et al., 2010], and Ionosonde-MS (Novosibirsk) [Podlesnyi et al., 2013].

By mutual agreement of the study participants, all ionograms for the analyzed dates were processed manually in order to avoid errors arising during automatic processing. Ionosonde measurement data from Juliusruh [https://giro.uml.edu/didbase/scaled.php] and Sodankylä [https://www.sgo.fi/Data/Ionosonde/ionData.php], taken from the websites, are presented in automatic processing options without manual verification. The time resolution of the experimental data was 15 min for ionosondes in Paratunka, Yakutsk, Zhigansk, Irkutsk, Norilsk, Ekaterinburg, Moscow, Juliusruh, and Sodankylä; half an hour for ionosondes in Tixie Bay, Salekhard, Lovozero; and 1 hour for ionosondes in Novosibirsk and Kaliningrad.

This work adopts a method of preparing and processing initial vertical sounding data, developed and analyzed earlier in [Shpynev et al., 2018]. This method has been repeatedly used for analyzing ionospheric disturbances from radiophysical measurements performed at mid- and high-latitude ionosonde chains [Chernigovskaya et al., 2021; Chernigovskaya et al., 2023, 2024a, b]). The primary data from ionosondes of various types was reduced to a common format for further processing. For each series of the initial data, the background values were calculated by averaging the experimental values of f_oF2(t) with a 27-day moving average over the smoothing interval of (t–14, t+14) days before and after each current hour t of the day. Then, series of deviations from the background level were calculated from time series of hourly initial data f_oF2(t). The relative deviations of the critical frequency, df_oF2(t) (in fractions of 1), were computed as deviations of current f_oF2(t) values from the background (averaged) level, related to the averaged value.

During the analyzed period of the magnetic storm from May 9 to May 15, 2024, there were periods of absence of measurement data for technical reasons: in Ekaterinburg (from 14:00 UT on May 11 to 02:30 UT on May 12, 2024; from 09:45 UT on May 13 to 08:15 UT on May 14, 2024); in Salekhard (from 11 to 13 UT on May 15, 2024); in Zhigansk (until May 11, 2024). In Yakutsk, the DPS-4 ionosonde worked very inconsistently, so measurement data is very fragmentary.

As in previous studies based on measurements of the mid-latitude ionosonde chain [Chernigovskaya et al., 2021; Chernigovskaya et al., 2024a, b], we use the F2-layer critical frequency f_oF2 [MHz] to analyze the effects of the magnetic storm in variations of the maximum electron density that is related to the maximum electron density in the F-region N_mF2 [m^{-3}] by the formula [Polyakov et al., 1968] $N_m\mathrm{F2} = 1.24 \cdot 10^{10} \left(f_o\mathrm{F2} \right)^2$.

To analyze the spatiotemporal variations in the neutral gas composition at ionospheric heights, we employ satellite measurements of [O]/[N_2] in the atmospheric gas column at heights above ~100 km, which are made by the optical method with the GUVI UV spectrometer on the TIMED spacecraft [Christensen et al., 2003; http://guvItImed.jhuapl.edu/guvi-galleryl3on2].

CHARACTERISTICS OF THE MAGNETIC STORM IN MAY 2024

The reason for the development of the May 10–12, 2024 strongest geomagnetic disturbance in the current century was the increased solar activity after a long period of low activity. From May 8 to May 11, 2024, several powerful solar flares occurred on the Sun in active region 3664: on May 8, 2024, a X1.0 flare and several M flares; on May 9, X2.25 and X1.12 flares; on May 10, a X3.98 flare; on May 11, at 01:23 UTC, another X-class flare of magnitude 5.4–5.7 [SWPC PRF 2541, 2024]. From May 10 to May 12, 2024, at least seven coronal mass ejections (CMEs) associated with the aforementioned solar flares [SWPC PRF 2541, 2024] reached Earth and caused a long severe geomagnetic storm. The passage of an interplanetary shock was recorded on May 10, 2024 at 16:39 UTC. For the rest of the day on May 10, the interplanetary magnetic field (IMF) B_z component was southward and occasionally decreased to –50 nT. The solar wind speed increased from 450 to 700 km/s with the arrival of the shock, reaching a maximum value ~1000 km/s on May 12 at 00:57 UTC [SWPC PRF 2541, 2024].

Figure 2 shows time variations in the geomagnetic and solar activity indices during the development of the magnetic storm in question. The magnetic storm began on May 10, 2024 at 17:00 UT; the time of the storm sudden commencement (SSC) is marked with the vertical dashed line denoted by S. By 21:00 UT, the intensity of the geomagnetic disturbance reached an extreme level (*Dst* from –200 to –350 nT according to the storm classification [Loewe, Prölss, 1997]) and category G4 (K_p=8 according to the NASA classification [https://www.swpc.noaa.gov/noaa-scales-explanation]), and an hour later, at 22:00 UT, the storm reached the class “great superstorm” (*Dst* below –350 nT) and category G5, extreme (see *Dst* and K_p plots in Figure 2). After midnight on May 10–11, the magnetic storm intensified to its maximum level and at 02:00 UT the *Dst* index dropped to –412 nT (indicted by the vertical dashed line designated by M in Figure 2), according to data from the World Data Center for Geomagnetism (WDC), Kyoto [https://wdc.kugi.kyoto-u.ac.jp/wdc/Sec3.html]. The K_p index reached 9, the A_p index rose to 400 nT at the peak of the storm. The storm main phase lasted ~9 hrs. It is worth mentioning that later, in 2025, on the WDC Kyoto website the *Dst* index was refined and corrected to –406 nT.

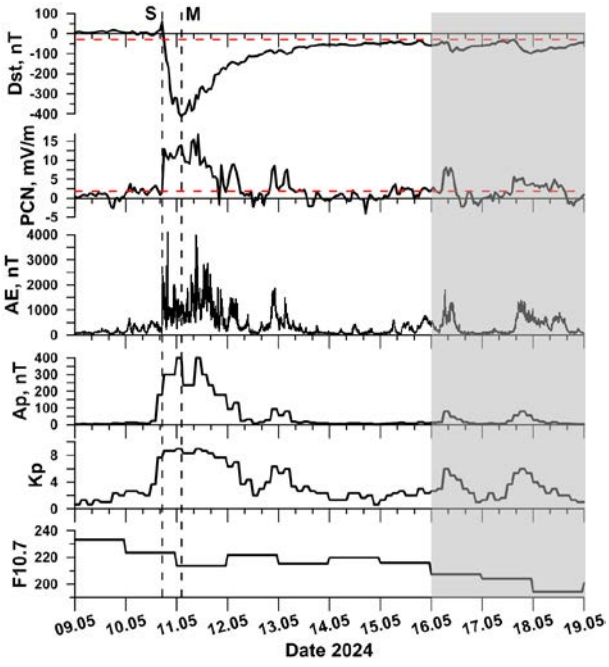

Figure 2. Variations in geomagnetic and solar activity indices. The threshold storm levels of *Dst* and *PCN* values are denoted by red horizontal dashed lines. Vertical dashed lines mark the moment of commencement of the storm (designated by S) and the moment of the maximum intensity of the magnetic storm (letter M)

Since in this work we analyze heliogeomagnetic effects of the mid- and high-latitude ionosphere, in addition to the geomagnetic indices *Dst*, K_p, and A_p we employ the indices of geomagnetic activity in the polar cap *AE* and *PCN* (see Figure 2). *AE* measures the magnetic disturbance caused by amplification of currents flowing along the auroral oval boundary in the ionosphere (eastward and westward polar electrojets). The unified *PC* index characterizes the magnitude of the geoeffective interplanetary electric field affecting the magnetosphere, as well as the solar wind dynamic pressure [Troshichev, Sormakov, 2018].

Noteworthy (see Figure 2) is the significant increase in *AE* to 4098 nT at 19:48 UT (according to data from the Department of Geophysics of AARI, St. Petersburg) and in *PCN* to 13–14 mV/m almost immediately after SSC at 17:00 UT with a further increase to 14 mV/ m at the peak of the storm (according to data from the World Data Center for Solar-Terrestrial Physics, Moscow [http://www.wdcb.ru/stp/geomag/geomagn_PC_ind.ru.html]). A significant increase in *PCN* indicates an increase in solar-wind storm drivers [Troshichev, Sormakov, 2018; Kalishin et al., 2020]. The close correlation between *PCN* and *AE* enhancements suggests that the interplanetary electric field and the solar wind dynamic pressure affect the ionosphere and magnetosphere in the polar region with high geoefficiency. This led to a significant amplification of currents flowing along the auroral oval boundary in the ionosphere — the eastward polar electrojet (*AE*>0).

Additional bursts of geomagnetic activity were detected during the storm recovery phase: at 9–10 UT on May 11, with the day changing according to Universal Time from May 11 to May 12 and from May 12 to May 13. These increases in geomagnetic activity are clearly seen in the *PCN*, *AE*, A_p, and K_p variations and are obviously related to the arrival of CMEs at Earth from a sequence of solar flares on May 9, 10, and 11, 2024 [SWPC PRF 2541, 2024]. No enhancement was recorded in *Dst* variations during these periods, which may be attributed to the geometry of solar wind streams. The rotation of active region 3664 from the Sun–Earth line after May 9 [SWPC PRF 2541, 2024] sent new coronal mass ejections away from Earth, and they only grazed Earth's magnetosphere.

The solar activity index *F*10.7 (radio emission flux with a wavelength of 10.7 cm (2800 MHz)) varied from 233 s.f.u. on May 09, 2024 to 216 s.f.u. on May 15, 2024 (1 s.f.u. (solar flux unit)=10^{-22} W·m^{-2}·Hz^{-1}) [http://www.wdcb.ru/stp/data/solar.act/flux10.7/daily/]. This corresponded to the growth phase of solar activity in solar cycle 25, which peaked in August 2024.

Threshold storm levels of *Dst*=–30 nT [Loewe, Prölss, 1997] and *PCN*~2 mV/m [Troshichev, Sormakov, 2018] are indicated by horizontal dashed lines in Figure 2. These levels show that the recovery phase of the superstorm lasted almost five days, until and including May 15, 2024. On May 16 and 17, new G2-level geomagnetic moderate storms occurred (gray shading in Figure 2); therefore, we analyzed the time interval until May 15, 2024 as related to this geomagnetic disturbance.

LONGITUDE-TIME VARIATIONS OF f_oF2 IN HIGH- AND MID-LATITUDE IONOSPHERE OVER EURASIA DURING THE VICTORY DAY 2024 GEOMAGNETIC STORM

Figure 3 illustrates longitude-time variations of the critical frequency f_oF2 measured at mid- (Figure 3, *a*) and high-latitude (Figure 3, *b*) ionosonde chains on May 9–15, 2024. Horizontal dashed lines on the maps of Figure 3, *a*, *b* denote the longitude of the ionosondes of high- (see Figure 1, Table 1) and mid-latitude (see Figure 1, Table 2) chains from the west of Eurasia to the east (from bottom to top respectively). Gray rectangles mark periods of data absence due to technical reasons or blackouts of ionosonde radio signals. Bottom panels (Figure 3, *c*) illustrate variations in the *Dst* and *PCN* indices during the magnetic storm. Red horizontal dashed lines depict the threshold levels of *Dst*<–30 nT and *PCN*>2 mV/m, starting from which geomagnetic conditions are classified as disturbed. Vertical dashed lines in the top and bottom panels denote the time of SSC (designated by S) and the maximum intensity of the storm (letter M).

When f_oF2 (and hence N_mF2) over Eurasia at middle (Figure 3, *a*) and high (Figure 3, *b*) latitudes is compared, the differences between the overall level of f_oF2 and the peak-to-peak amplitude of diurnal variations under quiet conditions (before the storm) are primarily noteworthy. This is due to the different seasonal lighting conditions at high and middle latitudes. The high-latitude ionosondes in Sodankylä, Salekhard, and Zhigansk are located at the latitude of the Arctic Circle (66.6° N), above which there is a polar day or a polar night. For high-latitude ionosondes, the analyzed period, May 9–15, 2024, is closer in terms of illumination conditions to the summer season than to the equinoctial one. At ionospheric heights, the Sun practically does not set in summer, which leads to a decrease in the manifestation of the transition of regular variations in ionospheric parameters from day to night. Accordingly, the diurnal variation of f_oF2 is much less pronounced than at the equinox. For midlatitudes, f_oF2 varied from 6–7 to 9 MHz (see Figure 3, *a*); for high latitudes, from 6 to 8 MHz (see Figure 3, *b*).

The variability in f_oF2 due to an increase in magnetic activity (under conditions of ionospheric storm development) in the high-latitude ionosphere is also lower than at midlatitudes, even in the case of such an extremely intense magnetic storm. Similar effects in the ionosphere at different latitudes were observed in [Araujo-Pradere et al., 2005; Chernigovskaya et al., 2021; Chernigovskaya et al., 2024a, b]. Araujo-Pradere et al. [2005], using a large array of observational data from 75 ionosondes covering a wide range of geomagnetic latitudes and including 43 storm intervals, statistically analyzed the variability in f_oF2 as a function of local time, latitude, season, and geomagnetic activity.

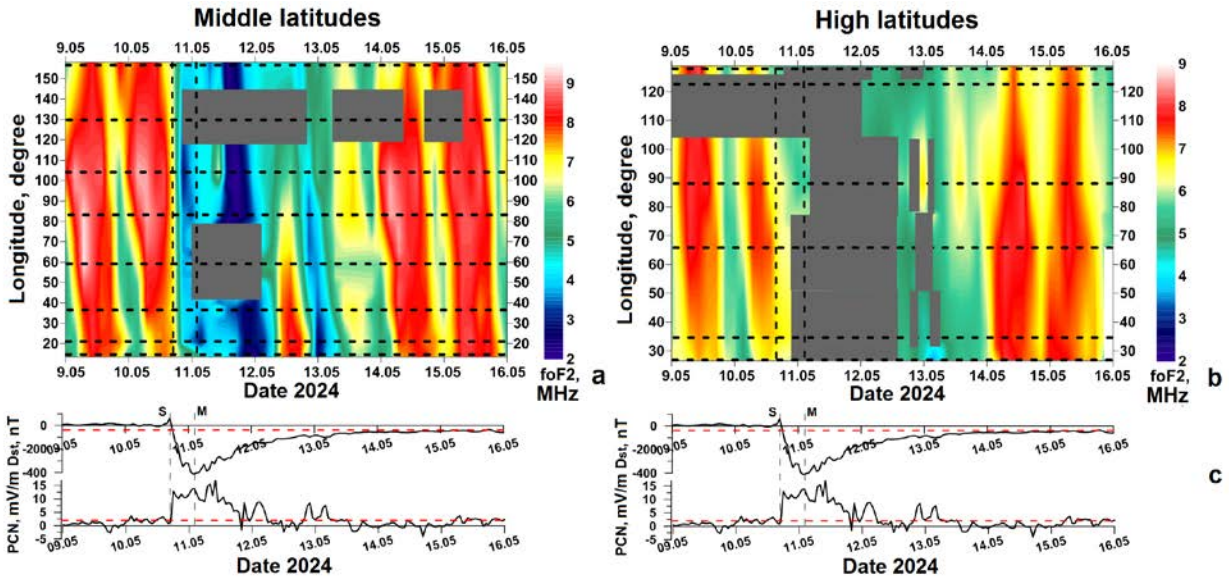

Figure 3. Longitude-time (UT) variations in the critical frequency f_oF2 according to the data from mid- (*a*) and high-latitude (*b*) ionosonde chains, as well as variations in the *Dst* and *PCN* indices (*c*)

According to the authors' conclusions, an unexpected result was that at high latitudes in all seasons the f_oF2 variability tended to decrease with increasing geomagnetic activity, probably due to an increase in the rising height of neutral molecular components and stronger chemical control of the ionosphere. In contrast to high latitudes, at middle and low latitudes the f_oF2 variability tended to increase with increasing geomagnetic activity in winter and during equinoxes and remained fairly constant in summer.

Almost immediately after SSC, on May 10, 2024 at 17:00 UT, as measured by all ionosondes regardless of the local time at the measuring point, a sharp drop in N_mF2 (and hence in f_oF2) was recorded at the height of the F2-layer maximum, which lasted throughout the storm main phase (see Figure 3, *a*, *b*). When the storm reached its maximum intensity at 02:00 UT on May 11, 2024 (*Dst*=–412 nT, vertical dashed line with letter M in Figure 3, *c*), f_oF2 decreased to 2–3 MHz according to data from mid-latitude ionosondes in Paratunka, Irkutsk, Novosibirsk, Moscow, Kaliningrad, and Juliusruh (see Figure 3, *a*). The DPS-4 ionosonde in Yakutsk worked very inconsistently after the onset of the geomagnetic storm (see Figure 3, *a*). When the magnetic storm reached maximum intensity, the ionosonde in Ekaterinburg showed a complete absence of data (so-called blackout). Then technical problems arose in operation of the Parus-3.0 ionosonde in Ekaterinburg (from 14:00 UT on May 11 to 2:30 UT on May 12, 2024) (see Figure 3, *a*).

Ionograms of almost all high-latitude ionosondes (except for the DPS-4 ionosonde in Norilsk) showed a complete absence of radio signals throughout the main phase of the magnetic storm (see Figure 3, *b*). Shortly after the maximum intensity of the storm, a blackout was also observed in data from the Norilsk ionosonde. Recall that the DPS-4 ionosonde in Zhigansk did not work for technical reasons until May 11, 2024.

An additional burst of geomagnetic activity at the midnight on May 11–12, recorded during the storm recovery phase in *PCN*, *AE*, A_p, and K_p variations (see Figures 2 and 3, *c*), was also accompanied by a significant decrease in the electron density at midlatitudes according to ionosonde measurements at all longitudes of the Eastern Hemisphere — over Paratunka, Irkutsk, Novosibirsk, Moscow, Kaliningrad, Juliusruh, except for Yakutsk and Ekaterinburg, where there were technical problems in ionosonde operation. It was an even longer negative ionospheric disturbance than that observed during the magnetic storm main phase, from noon on May 11 to ~06 UT on May 12. A decrease in f_oF2 to 2–3 MHz was recorded (see Figure 3, *a*), i.e. to the values detected during the main phase of the May 10–11, 2024 superstorm.

After that, according to ionosonde data from Ekaterinburg (f_oF2 to ~7 MHz), Moscow, Kaliningrad, and Juliusruh (f_oF2 to ~8 MHz) over the mid-latitude region of Eastern and Western Europe during the afternoon hours of May 12, 2024 under local daylight conditions, a temporary recovery in the electron density to the undisturbed level on May 9–10, 2024 took place (see Figure 3, *a*). However, the regions of Eastern Siberia and the Far East of Eurasia, where there were evening and night conditions, continued to be in the negative ionospheric storm phase (f_oF2~4–5 MHz, Figure 3, *a*).

Another burst of geomagnetic activity was detected at midnight on May 12–13, 2024 (*PCN*, *AE*, A_p, K_p in Figures 2 and 3, *c*). By this time, the *Dst* index had already risen to –98 nT (at 22 UT on May 12). This increase in geomagnetic activity, associated with the arrival of another coronal mass ejection at Earth from a sequence of solar flares on May 9–11, 2024, again led to a sharp drop in the electron density that recovered during the daylight hours on May 12, 2024. For several hours at the beginning of May 13, 2024 over the longitudes of Europe (according to the ionosonde data from Juliusruh, Kaliningrad, Moscow, Ekaterinburg) and Western Siberia (according to Novosibirsk ionosonde data), f_oF2 decreased to ~2–3 MHz (see Figure 3, *a*). At the longitudes of mid-latitude Eastern Siberia and the Far East, the effect of the negative ionospheric storm was observed throughout the storm main phase during early hours of May 11, 2024, and then in the recovery phase for the rest of the day on May 11, May 12, and the first half of May 13, i.e. two and a half days (see Figure 3, *a*).

When discussing the negative response in the mid-latitude ionosphere during geomagnetic disturbances, it is necessary to take into account the well-known effect of expansion and shift of ionospheric ionization troughs and other features of the high-latitude ionosphere from polar regions to the south. Boundaries of MIT and other ionospheric ionization troughs (ring, high-latitude, etc.), as well as particle precipitation zones, shift to midlatitude; electron density gradients on their boundaries increase; and sporadic ionospheric layers are formed. Mid-latitude ionosondes record subauroral ionograms during such periods [Mamrukov et al., 2000]. It is obvious that during the magnetic storm of interest MIT shifted further south of the geomagnetic latitudes 42°<GMlat<54° N, where ionosondes of the mid-latitude Eurasian chain are located [Danilchuk et al., 2025; Ponomarchuk et al., 2025]. This is confirmed by numerous visual observations of auroras in regions situated significantly south of these latitudes [Grandin et al., 2024].

From the second half of May 13, an increase in the electron density to the pre-storm level (f_oF2~7 MHz) began at all longitudes of mid-latitude Eurasia. At the end of the recovery phase of the May 14–15, 2024 magnetic storm, increased electron density was detected in the mid-latitude ionosphere over Eurasia (see Figure 3, *a*). Such an electron density increase can be attributed to the ionospheric aftereffect [Klimenko et al., 2018; Ratovsky et al., 2018].

Numerical calculations with GSM TIP (Global Self-consistent Model of the Thermosphere, Ionosphere and Protosphere) [Namgaladze et al., 1988; Klimenko et al., 2018] and statistical analysis of data from mid-latitude ionosondes in Irkutsk and Kaliningrad [Ratovsky et al.,

2018] have revealed that the cause of the positive electron density disturbances observed in the daytime a few days after the onset of the magnetic storm recovery phase might have been an increase in the atomic oxygen concentration due to its transfer from equatorial latitudes to midlatitudes during the late recovery phase [Klimenko et al., 2018]. In turn, this transfer is driven by an additional neutral gas pressure gradient from low latitudes to high latitudes, resulting from the appearance of excess neutral gas density at low latitudes during the geomagnetic storm main phase due to oxygen transfer from auroral latitudes toward the equator. In this case, the electron density may exceed the level of quiet days before the onset of a magnetic disturbance. The authors compare the [O]/[N_2] perturbation, as well as the electron density perturbation, with the oscillation of a pendulum, which passes from a negative phase to a positive one within a few days after the onset of the storm recovery phase.

The ionosondes of the high-latitude chain (Norilsk, Salekhard, Lovozero, Sodankylä) showed a complete absence of data (radio signal blackout) starting from the last hours of May 10 and the first hours of May 11, 2024 (the main phase of the storm) until the evening of May 12, 2024 (recovery phase), i.e. more than one and a half days (see Figure 3, *b*). The radio signal blackout period according to the ionosonde data from Tixie Bay was slightly shorter until the morning of May 12, 2024. The ionosonde in Zhigansk, which started operating at the beginning of May 12, 2024, showed very low f_oF2 (3.5–4 MHz) compared to the quiet days before the storm. Such a long period of radio signal blackout included periods of additional bursts of geomagnetic activity, as observed in *PCN*, *AE*, A_p, and K_p variations (see Figures 2 and 3, *c*) from the pre-noon hours of May 11 to ~06 UT on May 12, 2024. The radio signal blackouts according to ionosonde data may be caused by both a strong drop in the electron density in the F-region of the ionosphere and an abnormal increase in radio wave absorption in the lower ionosphere.

In the evening on May 12, 2024, all ionosondes of the high-latitude chain began to record low electron density values (f_oF2~4÷5 MHz; see Figure 3, *b*). Another burst of geomagnetic activity in the magnetic storm recovery phase at midnight on May 12–13, 2024 (*PCN*, *AE*, A_p, K_p in Figures 2 and 3, *c*) again led to a blackout of radio signals from ionosondes in Tixie Bay, Norilsk, Salekhard, Lovozero for several hours (see Figure 3, *b*), except for ionosondes in Zhigansk and Sodankylä. If, according to Sodankylä ionosonde data, a very low electron density was observed over Western Europe (f_oF2~3.5÷4 MHz) (see Figure 3, *b*), at the longitude of high-latitude Eastern Siberia the Norilsk ionosonde detected an increased electron density (f_oF2~6.5÷7 MHz; see Figure 3, *b*). Recall that during this period the electron density in the longitude sector of midlatitudes of Western Siberia, Eastern and Western Europe (see Figure 3, *a*) was also lower than at longitudes of Eastern Siberia and the Far East. In general, the effect of the negative ionospheric storm was observed over the high-latitude region of Eurasia, as well as over the mid-latitude region, for two and a half days — from the beginning of May 11 to the first half of May 13 inclusive (see Figure 3, *b*), i.e. the entire main phase and part of the recovery phase of the magnetic superstorm.

Since the second half of May 13, the electron density (f_oF2~6÷6.5 MHz) began to recover at the longitudes of Eastern Siberia and the Far East of high-latitude Eurasia. In the longitude sector of Western Siberia, Eastern and Western Europe (see Figure 3, *b*), the electron density was lower (f_oF2~5÷6 MHz). This difference may be related to the difference in local solar time, since the local day starts earlier in the eastern longitude sector than in the western one.

At the end of the recovery phase of the magnetic storm on May 14–15, 2024 at all longitudes of high-latitude Eurasia, the electron density began to increase to the pre-storm level (f_oF2~6.5÷7.5 MHz) (see Figure 3, *b*). There was a period of increased electron density in the high-latitude ionosphere (see Figure 3, *b*) when at night the electron density did not decrease to the values in undisturbed conditions before the onset of the superstorm. The peak-to-peak amplitude of diurnal variations in f_oF2 was only ~1 MHz (from 6.5 to 7.5 MHz), whereas before SSC the diurnal variation in f_oF2 was ~2.5 MHz (from 5 to 7.5 MHz; see Figure 3, *b*). Thus, at all longitudes of Eurasia in the high-latitude region (see Figure 3, *b*), as well as at midlatitudes (see Figure 3, *a*), the ionospheric aftereffect was clearly manifested [Klimenko et al., 2018; Ratovsky et al., 2018], with an electron density increase being more pronounced over the high-latitude region than over the mid-latitude region, which is unusual and very interesting. This raises the question about mechanism of this phenomenon. The authors [Klimenko et al., 2018; Ratovsky et al., 2018] believe that the electron density increase should occur earlier and be more pronounced at midlatitudes than at high latitudes during the ionospheric aftereffect of a magnetic storm. Analysis of spatiotemporal variations in f_oF2 based on measurement data from the high- and mid-latitude Eurasian ionosonde chains (see Figure 3, *a*, *b*) shows that the electron density began to rise on May 14, 2024 almost simultaneously at middle (see Figure 3, *a*) and high (see Figure 3, *b*) latitudes. Variations in thermodynamic parameters and thermospheric gas composition directly over high-latitude Eurasia during the magnetic storm recovery phase might have played a role here.

It must be borne in mind that the radio signal blackout in the ionograms of high-latitude ionosondes during the main and recovery phases of the magnetic storm results from the combined action of mechanisms of electron density decrease in the upper ionosphere (negative ionospheric storms, which are the dominant characteristic of the ionospheric response to increased geomagnetic activity) and an anomalous increase in radio wave absorption in the lower ionosphere. It is known that radio wave absorption in the ionosphere is proportional to the electron density and the frequency of electron-neutral particle collisions. During geomagnetic disturbances, both of these parameters can be very high in the lower ionosphere (D- and E-regions) due to penetration of energetic particles from the magnetosphere

into the high-latitude ionosphere along magnetic field lines, intense ionization, and plasma heating. Radio wave propagation to the F2-layer maximum ionization height can be hindered by sporadic E_s layers forming in the E-region (90–140 km). At high and middle latitudes, especially during magnetic disturbances, these layers appear quite often. As a result, the mid- and high-frequency radio waves used in vertical sounding are completely absorbed in the lower layers of the ionosphere. Therefore, to analyze the ionospheric effects of magnetic storms in more detail, it is necessary to additionally examine variations in the parameter f_{min}, which characterizes absorption of radio waves in the lower ionosphere in the D-region, as well as the parameter f_oE_s that describes the formation of sporadic layers in the E-region, which shield radio signals. Detailed analysis of variations in these ionospheric parameters based on measurements of the Eurasian ionosonde chains during the May 2024 superstorm is performed in [Chernigovskaya et al., 2026].

SPATIOTEMPORAL VARIATIONS OF [O]/[N_2] IN THE THERMOSPHERE DURING THE VICTORY DAY 2024 GEOMAGNETIC STORM

To explain the spatiotemporal variations in the electron density of the ionosphere in the F2-region, recorded during the May 2024 superstorm, Figure 4 presents maps of longitude-time variations in the relative deviations of the critical frequency f_oF2 derived from mid-latitude ionosonde chain data (Figure 4, *a*) and in [O]/[N_2] in the atmospheric gas column in the thermosphere (ionosphere) above ~100 km for mid-latitude Eurasia (54°–56° N) (Figure 4, *b*) according to satellite measurements with the GUVI/TIMED UV spectrometer [Christensen et al., 2003]. Analysis of relative deviations df_oF2 allows us to very clearly assess the degree of impact exerted by the geomagnetic disturbance during the storm as compared to the undisturbed electron density on quiet days before the onset of the geomagnetic disturbance (the SSC time is indicated by the vertical dashed line on the distribution map and denoted by S in Figure 4, *c*). Moreover, such an analysis makes it possible to eliminate the possible ambiguity in identifying the ionospheric parameter in ionosondes of different types.

Unfortunately, there is no satellite data on [O]/[N_2] for high-latitude Eurasia (60°–65° N) probably due to peculiarities of the TIMED satellite's orbit inclination or technical measurement problems. The physical parameter [O]/[N_2] is a good indicator of negative phases of ionospheric storms [Prölss, Werner, 2002; Laštovička, 2002; Danilov, 2003; Liou et al., 2005]. A decrease in [O]/[N_2] in the thermospheric gas leads to a decrease in the electron density in this region and hence to the development of a negative ionospheric storm.

Complex and intense electrodynamic processes occurring under conditions of the superstorm at polar latitudes (see *AE* variations in Figure 4, *c*) caused a very strong decrease in [O]/[N_2] at thermospheric heights over all longitudes of mid-latitude Eurasia in the range 54°–56° N (Figure 4, *b*), coinciding with the location of the mid-latitude chain's ionosondes. By analyzing the longitude-time variations in df_oF2 at midlatitudes of the Eastern Hemisphere from ionosonde measurements (see Figure 4, *a*) and variations in neutral composition at the same latitudes and longitudes (Figure 4, *b*) from satellite measurements, we can conclude that when visually compared these parameters demonstrate a very high level of similarity, which indicates a high positive correlation. The longitude-time distribution of [O]/[N_2] explains in detail the previously described features of the

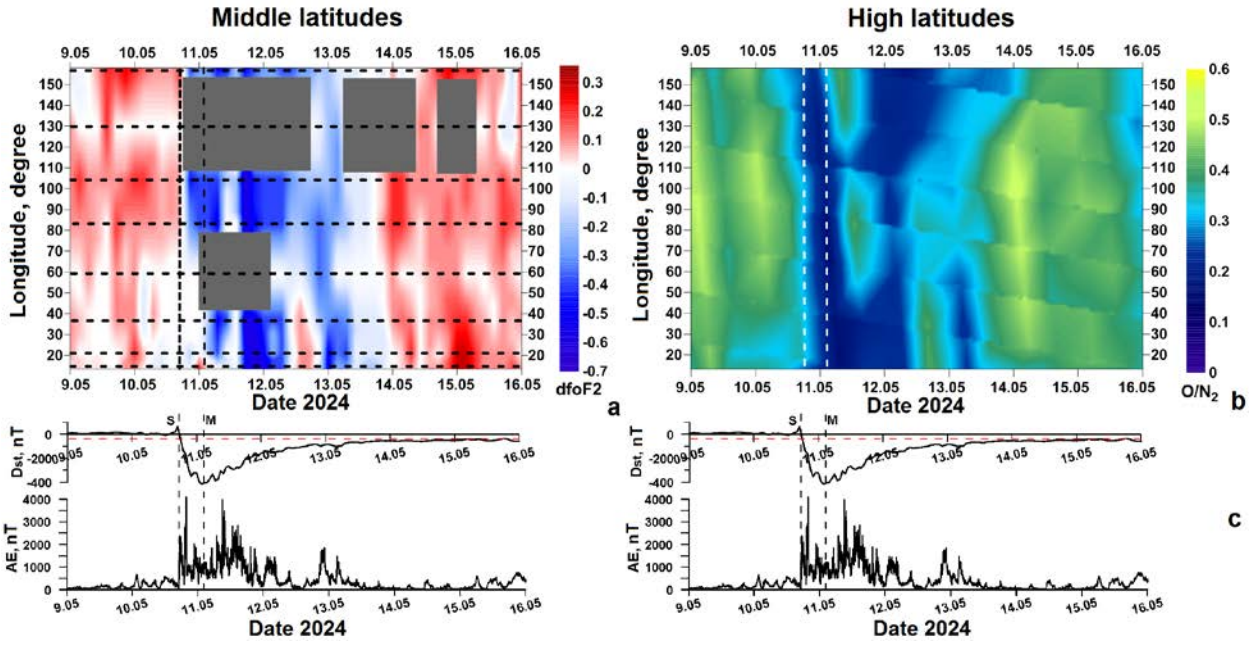

Figure 4. Longitude-time variations in df_oF2 according to data from the mid-latitude ionosonde chain (*a*) and the ratio [O]/[N_2] as measured by GUVI TIMED for the mid-latitude region (*b*) in May 2024 (UT), as well as variations in the *Dst* and *AE* indices (*c*)

ionospheric plasma response to the extreme geomagnetic disturbance. First, there was a sharp and strong decrease in f_oF2 in the ionosphere of mid-latitude Eurasia, which was observed almost from the moment of the sudden commencement of the magnetic superstorm, which ranged from 50 to 70 % of f_oF2 under quiet conditions, smoothed by a 27-day moving average. The negative ionospheric storm lasted for the entire main phase and more than two days, until the evening of May 13, 2024, during the magnetic storm recovery phase. During the negative ionospheric storm, the [O]/[N_2] ratio was very low (0.1–0.2), increasing in some short periods to 0.3÷0.4, for almost three days — from the evening of May 10 to the evening of May 13, 2024.

After the storm main phase ended, over the Far East (120–150 °E) on May 11, 2024 (LT) a region of [O]/[N_2] increased to 0.3÷0.4 was formed. This region was slowly moving westward toward Eastern and further Western Siberia (50–100° E) during the local daytime on May 11, 2024. This westward motion of the region of high (or low) [O]/[N_2] due to the increased neutral wind as a result of heating of neutral gas in the lower thermosphere during the storm main phase is similar to the motion of a wave-like disturbance of molecular gas. Similar westward wave-like disturbances of thermospheric molecular gas were reported in [Chernigovskaya et al., 2021], where the ionospheric response to the St. Patrick's Day extreme magnetic storm in March 2015 was analyzed.

Additional bursts of geomagnetic activity observed in *PCN*, *AE*, A_p, and K_p variations (see Figures 2 and 4, *c*) during the storm recovery phase, accompanied by significant decreases in electron density at midlatitudes, as measured by ionosondes at all longitudes of the Eastern Hemisphere (see Figures 3, *a*, 4, *a*), were clearly associated with the corresponding periods of low [O]/[N_2] (see Figure 4, *b*). It was a long-lasting negative ionospheric disturbance — from noon on May 11 to ~06 UT on May 12. A drop in f_oF2 to 2–3 MHz (see Figure 3, *a*) and in relative deviations df_oF2 to –0.5÷–0.7 (see Figure 4, *a*) was recorded over Paratunka, Irkutsk, Novosibirsk, Moscow, Kaliningrad, and Juliusruh, except for Yakutsk and Ekaterinburg, where there were technical problems in ionosonde operation. There was a decrease in the electron density to the values observed during the main phase of the superstorm on May 10–11, 2024.

After that, during the local day on May 12, 2024, a temporary increase in the electron density occurred over mid-latitude Western Europe (according to ionosonde data from Juliusruh and Kaliningrad) and Eastern Europe (according to ionosonde data from Moscow and Ekaterinburg) to the undisturbed level on May 9–10, 2024 (f_oF2 to ~8 MHz, see Figure 3, *a*; df_oF2 to 0.1÷0.3, see Figure 4, *a*). This local increase in the electron density in the limited longitude sector is clearly related to the increase in [O]/[N_2] in the same latitude-longitude region during the local day (see Figure 4, *b*). Apparently, changes in the composition of the neutral thermosphere at heights above 100 km might have been associated with a decrease in the strength of currents flowing along the auroral oval boundary in the ionosphere (eastward and westward polar electrojets), whose variability is indicated by *AE* variations (see Figure 2). However, the regions of Eastern Siberia and the Far East of Eurasia, where evening and night conditions were present, continued to be in the negative ionospheric storm phase: f_oF2~ 4–5 MHz (see Figure 3, *a*) and df_oF2 to –0.3÷–0.5 (see Figure 4, *a*).

Another burst of geomagnetic activity was recorded at midnight on May 12–13, 2024 (see *PCN*, *AE*, A_p, K_p in Figures 2 and 4, *c*) when the *Dst* index had already risen to –98 nT (on May 12 at 22 UT). This increase in geomagnetic activity, linked to the arrival of another coronal mass ejection at Earth from a sequence of solar flares on May 9–11, 2024, again led to a sharp drop in the electron density over Europe, which recovered during the daytime on May 12, 2024 (see Figure 3, *a*, Figure 4, *a*). Approximately until noon on May 13, 2024 over the longitudes of Europe (according to ionosonde data from Juliusruh, Kaliningrad, Moscow, Ekaterinburg) and Western Siberia (according to Novosibirsk ionosonde data), f_oF2 decreased to ~2–3 MHz (see Figure 3, *a*); and df_oF2, to –0.4÷–0.6 (see Figure 4, *a*). This decrease in the electron density in the F2 layer was caused by another decrease in [O]/[N_2] (see Figure 4, *b*) over all longitudes of mid-latitude Eurasia. The lowest ever values of [O]/[N_2] were recorded in the longitude sectors of mid-latitude Western and Eastern Europe, as well as over the Far East.

At the longitudes of mid-latitude Eastern Siberia and the Far East, the effect of the negative ionospheric storm was observed throughout the main phase of the storm in the early hours on May 11, 2024, and then for the rest of the day on May 11, May 12, and the first half of May 13, i.e. for two and a half days during the recovery phase of the magnetic storm (see Figure 3, *a*). The values of df_oF2 varied at different longitudes from –0.2 to –0.5 (see Figure 4, *a*). This long-lasting negative perturbation of the electron density, covering a vast Asian territory, was triggered by an extraordinary catastrophic drop in [O]/[N_2] for almost three days during the superstorm (see Figure 4, *b*), as measured by GUVI/TIMED.

Then, from the second half of May 13, 2024 at all longitudes of mid-latitude Eurasia, the electron density began to increase to the pre-storm level df_oF2~0÷0.3 (see Figure 4, *a*). The electron density increase was associated with the increase in [O]/[N_2] throughout mid-latitude Eurasia (see Figure 4, *b*).

Figure 5 presents a sequence of maps of the global spatial distribution of [O]/[N_2] in the Northern Hemisphere at thermospheric heights above ~100 km for each day from May 10 to May 15, 2024 [http://guvitimed.jhuapl.edu/guv i-galleryl3on2], which allows the dynamics and transformation of large-scale regions of reduced [O]/[N_2] to be visually traced from day to day. The maps show that with the onset of the superstorm in the evening (UT) on May 10, 2024 during the main phase of the storm on May 10–11 and then during the storm recovery phase until the end of May 11, a giant region of very low [O]/[N_2] covered the Northern

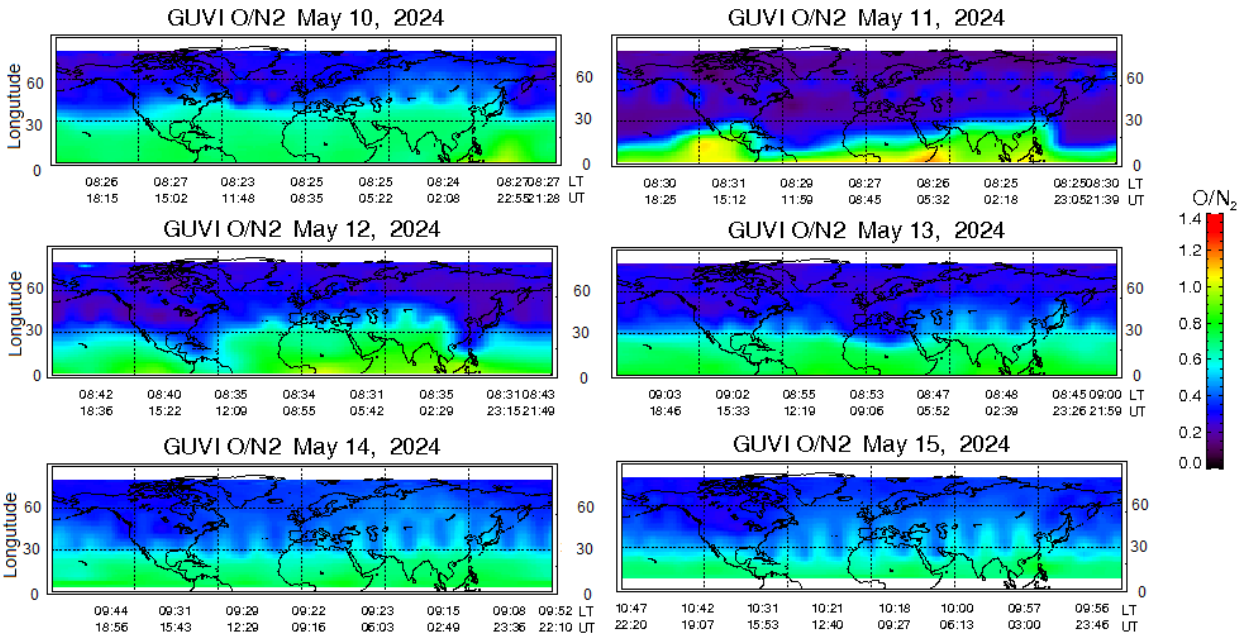

Figure 5. Global spatial distribution of [O]/[N_2] in the Northern Hemisphere at thermospheric heights above ~100 km measured by GUVI/TIMED for each day from May 10 to May 15, 2024

Hemisphere from high to near-equatorial latitudes (~0.1–04) at heights above ~100 km. The regions of extreme thermospheric gas penetration with low [O]/[N_2] to the equator (latitudes lower than 10° N) on May 11 were located over the Pacific and Atlantic Oceans; and on May 12, 2024, they shifted to the west, covering the territories of the Far East of Eurasia and North America. In the longitude sectors of the Northern Hemisphere over Eurasia and the Atlantic Ocean, the boundary of low [O]/[N_2] rose to 30°÷40° N. Over the central Pacific Ocean, the boundary of low [O]/[N_2] remained at latitudes of ~25° N (i.e., at the latitude of the Northern Tropic). By May 13, 2024, the boundary of low [O]/[N_2] was still at ~30° N for almost all longitudes. Only over Africa, the region of low [O]/[N_2] had a protrusion up to ~25° N. It is appropriate to recall here that on May 12–13, 2024 bursts of geomagnetic activity were recorded which might have caused variations in the spatial distribution of [O]/[N_2].

On May 14, 2024, we could observe a gradual increase in [O]/[N_2] (to 0.5÷0.7) over midlatitudes of Eurasia, which showed up in the electron density rise at the F2-region height on May 14–15, 2024, recorded by midlatitude ionosondes (Figure 4, *a*).

SPATIOTEMPORAL VARIATIONS OF [O]/[N_2] IN THE THERMOSPHERE DURING SUPERSTORMS IN OCTOBER–NOVEMBER 2003

It is of great interest to compare the intensity of the response of the thermospheric neutral gas composition during the strongest geomagnetic events of the 21st century. GUVI/TIMED measurements of [O]/[N_2] for thermospheric heights above 100 km have been published on the website [https://guvitimed.jhuapl.edu/guvi] since the end of February 2002. Thus, we can compare the spatiotemporal variations in [O]/[N_2] during the magnetic storm in May 2024 (Figure 5), analyzed in this paper, and during the strongest magnetic storms of the first two decades of the 21st century, observed in the fall of 2003 (Figure 6): October 29–31 (Halloween storm) with *Dst*=–401 nT (top panels) and November 20 with *Dst*=–472 nT (bottom panels) [Gopalswamy et al., 2005]. These magnetic storms are classified as superstorms according to *Dst* [Loewe, Prölss, 1997] and fall in the category G5, extreme according to the NASA classification based on K_p [https://www.swpc.noaa.gov/noaa-scales-explanation].

Comparison between spatial distributions of [O]/[N_2] at thermospheric heights above ~100 km in the Northern Hemisphere according to GUVI/TIMED data during the October and November 2003 superstorms (see Figure 6) and during the May 2024 superstorm (see Figure 5) suggests that the response of the thermospheric neutral gas composition to the processes developing at high latitudes of the Northern Hemisphere on May 10–15, 2024 was more global, with penetration of thermospheric disturbances at almost all longitudes up to near-equatorial latitudes (~10° N) and with very low [O]/[N_2] ~0.1÷0.4.

During the October 29–31, 2003 superstorm when the *Dst* index decreased to –401 nT, the main region of decreased [O]/[N_2] was formed over the Atlantic Ocean and the east coast of North America (top panels in Figure 6). Above this longitude region, the boundary of decreased [O]/[N_2] dropped to ~30° N on October 20–30 and even lower, to ~20° N, on October 31, 2003. At other longitudes of the Northern Hemisphere, the region of low [O]/[N_2] reached midlatitudes 50°–60° N.

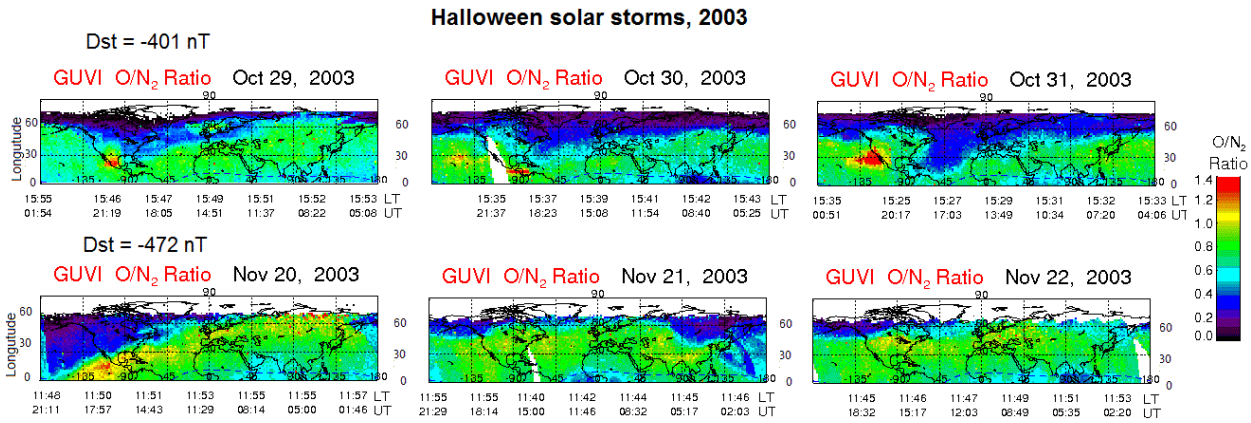

Figure 6. Global spatial distributions of [O]/[N_2] at thermospheric heights above ~100 km in the Northern Hemisphere measured by GUVI/TIMED on October 29–31 (top panels) and November 20–22, 2003 (bottom panels) during superstorms

During the November 20, 2003 superstorm when the *Dst* index decreased to –472 nT, the thermospheric gas reaction at different longitudes of the Northern Hemisphere was not global either. According to GUVI/TIMED data, the expansion of the region of significantly decreased [O]/[N_2] up to near-equatorial latitudes was observed only for the longitude region of the western Pacific Ocean and North America at latitudes above 30° N (bottom panels in Figure 6). On the next day, November 21, 2003, the region of low [O]/[N_2] shifted to the west and was located over the eastern Pacific Ocean and over the Far East and Eastern Siberia.

Due to such strong differences in spatiotemporal variations of thermospheric composition during the most extreme geomagnetic storms of the 21st century (Figures 5, 6), it is interesting to compare the ionospheric response at different longitudes and latitudes of the Northern Hemisphere to such intense geomagnetic disturbances. Unfortunately, we do not have measurement data on the magnetic superstorms in October–November 2003 from the Eurasian ionosonde chains, so we use the results of ionospheric response studies published by our colleagues in scientific periodicals.

Blanch et al. [2005] have analyzed ionospheric effects for superstorms in October–November 2003, employing data from European ionosondes in Chilton (51.5° N, 359.4°E), Průhonice (50.0° N, 14.6°E), and El Arenosillo (37.1° N, 353.3°E), and also from GPS receivers. The authors note that despite the extremely high solar wind speed on October 29–30, 2003 (1850 km/s) the relatively low proton density led to a moderate solar wind dynamic pressure that is proportional to the solar wind plasma speed and density. Due to the moderate solar wind dynamic pressure and the IMF short-term negative B_z component, the October 2003 event, contrary to expectations, was not unusually geoeffective. The November 20, 2003 geomagnetic storm, more intense according to the *Dst* index (–470 nT), became a more significant event in terms of its impact on Earth's ionosphere in the European mid-latitude sector, although for this event the solar wind speed was much lower than that for the October storm, only 750 km/s. The authors note that two ionospheric effects were recorded during the November 2003 superstorm: 1) the presence of well-developed anomalous disturbed E_s layers at latitudes up to 37° N; 2) the formation of two thin separate latitudinal belts of decreased (negative effect in the range 55–45° N) and increased (positive effect in the range 45–30° N) electron densities in the European dusk sector during the storm main phase (Blanch et al., 2005).

Kane [2005] has analyzed the global ionospheric response for the October 2003 superstorm, using data from 83 ionosondes from the NGDC SPIDR website [http://spidr2.ngdc.noaa.gov/spidr/]. Electron density troughs (negative ionospheric storms) were detected at high northern and southern latitudes. At northern middle and low latitudes, very strong positive effects were recorded in the spatial distribution of the electron density on October 29, 2003, followed by negative effects the next day. During the November 2003 superstorm, there were no electron density troughs at northern high latitudes during morning and evening hours, but they were observed at night. For middle and low latitudes, strong negative effects were seen at some longitudes in the early morning, as expected, yet some longitudes featured strong positive effects at noon and in the evening. Thus, there were many deviations from model prognostic estimates. The deviations were irregular, indicating significant local ionospheric effects overlapping with general patterns. A puzzling feature was the presence of strong positive effects within 24 hours before the storm.

Uma et al. [2012], using ionospheric parameters from ionosondes and global ionospheric maps of total electron content (GIMs TEC), measured by ground GPS receivers, as well as in-situ electron density measurement data from the Planar Longmuir probe on board the CHAMP satellite, have examined the role of the electric field (measured indirectly) and thermospheric wind (from the empirical disturbed wind model) in the ionospheric response over the Japanese and Indian longitude sectors during the November 20, 2003 geomagnetic superstorm. A significant expansion and intensification of the equatorial ionization anomaly was detected during the main phase of the storm, which, as the authors believe, were caused by prompt penetration electric fields (PPEFs), often observed at equatorial latitudes.

Furthermore, the storm-associated equatorward thermospheric wind (with an average speed of ~230 m/s) during the recovery phase of the storm caused the F-layer virtual height (*h*'F) to rise with a constant time delay, starting at midlatitudes and then spreading to low and equatorial latitudes.

The negative effect of the ionospheric storm was found in measurement data on f_0F2 from mid- and low-latitude ionosondes WKA (45.21°N, 141.11° E), KOB (35.41° N, 139.291° E), and YAG (31.21° N, 130.371°E). At the same time, data from the near-equatorial ionosonde WTR (17.71° N, 83.31° E) pointed to a positive effect of the ionospheric storm; and data from the TRV ionosonde, even closer to the equator (8.51° N, 771° E), again to a negative effect in the electron density at the F2-layer height during the main phase of the November 2003 geomagnetic storm [Uma et al., 2012]. GIMs TEC, which also fairly well reflected these longitude-latitude features of the ionospheric response, showed a latitudinal expansion (only to ~25° N) and intensification (by ~80–100 TECU) of the equatorial ionization anomaly. The presence of PPEFs was revealed in both longitude sectors during the main phase of the superstorm, which is confirmed by data from ground-based magnetometers.

Even the above brief overview of the results of the analysis of the October–November 2003 superstorms' ionospheric effects indicates that there are significant differences in the ionospheric response to extreme geomagnetic disturbances in October–November 2003 and May 2024: the ionospheric response in the Northern Hemisphere to geomagnetic storms in October–November 2003 was not as uniform and global as the response to the storm in May 2024.

DISCUSSION

The first thing that can influence the character of development of magnetic storms, and then ionospheric effects associated with geomagnetic disturbances, is always the individual characteristics of solar activity, conditions in the solar wind (speed, pressure), and the behavior of geomagnetic indices during magnetic storms. They are different, and this must be borne in mind. In this study, we did not examine this issue in detail, since the analysis was conducted for a different purpose.

Ionospheric storms in October–November 2003 in different latitude and longitude regions occurred under diverse scenarios — with a change of the primary positive ionospheric storm effect to the negative one (at midlatitudes of Europe), with only a negative or positive effect (at high and low latitudes of Eurasia). The ionospheric response to the May 2024 storm featured a negative effect at all longitudes of Eurasia from high to near-equatorial latitudes.

The reason for the different ionospheric responses lies in the physical mechanisms that became predominant during the events considered. During the October–November 2003 superstorms, PPEFs played a significant role, forming a giant plasma fountain (dayside ionospheric super fountain) that transports plasma from the equatorial region to higher altitudes and higher latitudes [Tsurutani et al., 2004; Astafyeva, 2009]. PPEFs are responsible for the positive phases of ionospheric storms observed at low and mid-low latitudes [Danilov, 2013]. Positive ionospheric storms are also caused by an increase in equatorward neutral winds resulting from the energy input to auroral latitudes during a magnetic storm [Prölss, 1995]. When positive ionospheric storms occur, the effects of neutral winds prevail over changes in the chemical composition at midlatitudes. This is clearly seen from the comparison between space-time distributions of [O]/[N_2] for the magnetic storms in October–November 2003 (Figure 6) and in May 2024 (Figure 5).

Negative ionospheric storms are the dominant characteristic of the ionospheric response to increased geomagnetic activity and are generally related to an equatorward shift of the MIT region [Prölss, 1995; Rishbeth, 1998]. Seaton [1956] was the first to suggest that a decrease in the electron density may be caused by variations in the thermospheric neutral gas composition. Enhancement of the westward auroral electrojet at high latitudes induces neutral winds, which redistribute the neutral atmospheric composition over most of the high-latitude region and part of the mid-latitude region. Oxygen, as a lighter gas, is faster transferred than nitrogen. This leads to a decrease in [O]/[N_2] in the upper atmosphere and hence to negative electron density disturbances in the F-region of the ionosphere [Mayr, Volland, 1972; Laštovička, 2002; Prölss, Werner, 2002; Danilov, 2003; Liou et al., 2005; Klimenko et al., 2011]. It is the predominant effect of this mechanism that we can see in the conditions of development of the May 2024 storm.

Comparing the significantly different responses of the ionosphere to magnetic superstorms of approximately the same intensity in October–November 2003 and May 2024, we can assume that seasonal differences in scenarios for development of ionospheric effects during geomagnetic disturbances played a role in this. The scenario of the ionospheric response with a positive ionospheric storm changing to a negative one (as for the superstorms in October–November 2003) is often observed for the equinox periods [Burešová et al., 2007; Ratovsky et al., 2020]. A similar scenario of ionospheric response over the middle and high latitudes of Eurasia during the equinox was intrinsic to the extreme, most intense magnetic storm of solar cycle 24 in March 2015 [Chernigovskaya et al., 2021; Chernigovskaya et al., 2024a], as well as to the strong magnetic storms in March 2012 [Chernigovskaya et al., 2023] and October 2016 [Chernigovskaya et al., 2024b].

The ionospheric response to the May 2024 magnetic storm seems to develop under the summer scenario when the negative ionospheric storm effect is predominant [Burešová et al., 2007; Ratovsky et al., 2020]. The same ionospheric response in the form of a negative ionospheric storm was recorded by Eurasian high- and mid-latitude ionosondes to the extreme geomagnetic disturbance in June 2015 [Chernigovskaya et al., 2021; Chernigovskaya et al., 2024a].

Measurements of ionospheric plasma parameters with the Irkutsk Incoherent Scatter Radar (IISR, 53° N, 103° E) and the vertical sounding ionosonde DPS-4 (52° N, 104° E) were carried out from May 10 to May 16, 2024. A multiple decrease in the electron density in the F2 layer (250–300 km) was clearly visible. On May 11, when the intensity of the storm was at its maximum, an almost fivefold decrease in the electron density in the F2 layer was recorded during the daytime relative to the period before the storm. There was also a rise in the height of the maximum electron density (to 400 km) at midnight on May 10–11 and a drop in the height of the maximum (below 200 km) in the afternoon on May 11 and 12 [Yasyukevich et al., 2025]. Similar effects were observed in the American sector [Themens et al., 2024]. The effects in the high-latitude ionosphere during the May 10–11, 2024 geomagnetic storm were examined by analyzing TEC variations along with incoherent scatter radar and ionosonde data. During the initial phase of the magnetic storm, plasma rose significantly. The height of ionization maximum increased by 150–300 km, reaching 630 km. Strong heating and change in the composition of the high-latitude thermosphere led to complete absence of the F2 layer on May 11, 2024 [Themens et al., 2024].

Chernyshov et al. [2025] have analyzed in depth the impact of the Victory Day 2024 magnetic storm on the subauroral and mid-latitude ionosphere (in particular, over the Kaliningrad region of Russia), using different instruments and observation methods. The study is based on data from satellite systems (Swarm, DMSP, TIMED), ground-based magnetometers, ionosondes, VLF receivers, GNSS receivers, and all-sky cameras. DMSP/SSUSI and an all-sky camera at Ladushkin ionosonde station in the Kaliningrad Region monitored changes in the auroral oval boundary during intense geomagnetic activity. During the storm over the Kaliningrad Region, such phenomena as STEVE and SAR arcs must have been observed. Thus, Kaliningrad was located inside the auroral oval, which is an extremely rare event. The auroral region of the increase in the ROTI index shifted to 45°/40° N during the main phase of the storm. Changes in the upper atmosphere: peak values of the cooling rate of nitric oxide NO, variations in TEC and $[O]/[N_2]$, according to the authors, indicate a significant impact on the thermosphere and ionosphere, confirming the theory of thermospheric-ionospheric storms. A decrease in $[O]/[N_2]$ (to three times) and TEC (to two times) denotes a long-term effect of geomagnetic activity on the structure of the upper atmosphere. The ionosonde data from Kaliningrad and the characteristics of VLF signal propagation have confirmed significant changes in the ionosphere at night on May 10–11, 2024, indicating that such powerful geomagnetic storms can cause failures and malfunctions in radio communications.

Kwak et al. [2024] during the May 2024 magnetic storm observed significant disturbances in the upper atmosphere both globally and locally over the Far Eastern sector of Asia in space and ground-based observations. Ground-based observations showed significant effects of negative ionospheric storms in the East Asian sector, including the Korean Peninsula, which are associated with heating of the thermosphere and with a decrease in $[O]/[N_2]$ in high-latitude regions. Strong variations in the components of the surface geomagnetic field related to the reaction to PPEFs during the magnetic storm were observed with magnetometers over the East Asian longitude region.

Spogli et al. [2024] have investigated ionospheric and geomagnetic effects occurring over the Mediterranean sector during the May 2024 magnetic superstorm, paying special attention to Italy. Networks of GNSS receivers, ionosondes, and magnetometers in the Mediterranean region were employed for the analysis, which contributed to detailed analysis of variations caused by the storm. Observatories located in Italy recorded maximum changes in geomagnetic field components ~600 nT. The most noticeable ionospheric effect after the onset of the magnetic disturbance was a significant decrease in the electron density on May 11, which led to a pronounced negative ionospheric storm, recorded in variations both in f_0F2 and TEC. The authors attribute the recorded effects to a decrease in $[O]/[N_2]$ in the thermospheric gas. The negative ionospheric storm effect was also detected on May 13, 2024.

Bojilova et al. [2024] have examined in depth the temporal evolution of spatial irregularities associated with the ionospheric response to the May 10–11, 2024 geomagnetic storm. For the analysis, ionospheric anomalies were used which were represented by positive and negative relative deviations of global TEC data, whose variations were studied depending on magnetic latitude, local time, and the behavior of geomagnetic activity parameters during the event in question. Special attention was paid to the analysis of the observed differences between ionospheric responses at low, middle, and high latitudes in the Northern and Southern hemispheres, taking into account the known mechanisms of the geomagnetic storm effect on the electron density. In the Northern Hemisphere at the beginning of the magnetic storm, an almost instantaneous negative electron density response appeared (under summer conditions), which spread to 30° N and gradually weakened by the end of May 11, 2024. In the Southern Hemisphere (under winter conditions) at latitudes south of 50° S at the beginning of the magnetic storm, a region with a predominantly positive electron density response was formed which changed to negative after midnight on May 11. The authors explained the recorded symmetric ionospheric response in the regions from the equator to latitudes 40° N and 40° S by the expansion of the strong equatorial ionospheric anomaly formed during the main phase of the magnetic storm. An interesting result of this study is the identification of the longitude structure of the negative ionospheric response at midlatitudes. It arose from the superposition of the structure of the negative ionospheric anomaly, associated with heated air propagation from the polar oval to low latitudes, on the structure of the positive ionospheric anomaly caused by the disturbed equatorial dynamo effect. Such a superposition could provoke different responses of the mid-latitude ionosphere in various longitude sectors.

A similar feature of the mid-latitude ionosphere response during a magnetically disturbed period, i.e. switching between the positive and negative phases of an ionospheric storm, was pointed out in [Habarulema et al., 2016; Chernigovskaya et al., 2023] for various longitude regions at midlatitudes of the Northern Hemisphere during a series of magnetic storms in March 2012. The authors attributed the change in ionospheric storm effects during the analyzed period to the superposition of competing processes in the mid-latitude region that affect ionospheric ionization, the sources of which are situated in the auroral ionosphere (a series of intense solar activity events that caused geomagnetic storms on March 7, 9, 12, and 15, 2012 and significant disturbances in the high-latitude atmosphere and ionosphere), as well as in the equatorial ionosphere (super-fountain effect at near-equatorial latitudes on March 7–10, 2012).

Ponomarchuk et al. [2025] have examined the effects of the May 10–13, 2024 extreme magnetic storm in Asian Russia by analyzing data from vertical and oblique sounding of the ionosphere with a continuous chirp signal. Features of ionospheric dynamics caused by the magnetic storm were revealed: prolonged negative ionospheric disturbance, manifested as a significant decrease in F2-layer critical frequencies and maximum observed frequencies of radio paths; shielding of reflections from the F-region by the E_s layer, and increased absorption of HF signals. The relationship of variations in ionospheric parameters and the maximum observed frequencies of HF radio wave propagation modes with the spatial position of MIT and the equatorial edge of the diffuse electron precipitation zone was established. According to the results of modeling of the invariant latitude of the MIT bottom by the model [Deminov, Shubin, 2018], Novosibirsk and Irkutsk ionosondes on May 10–13, 2024 were located at latitudes south of the polar wall or the MIT bottom in the dusk and night local time sectors. This is supported by the results of reconstruction of the location of the polar oval from DMSP/SSUSI data [https://ssusi.jhuapl.edu/gal_edr-aur_cs].

CONCLUSIONS

Study of the ionospheric response to the Victory Day 2024 extreme geomagnetic storm based on the analysis of data from mid- and high-latitude Eurasian ionosonde chains, as well as GUVI/TIMED measurements of $[O]/[N_2]$ in the thermospheric gas column at heights above ~100 km allowed us to draw the following conclusions:

1. When comparing longitude-time distributions of f_oF2 (and hence N_mF2) for mid- and high-latitude Eurasia, primarily noteworthy are the differences between the overall level of f_o F2 and the peak-to-peak amplitude of diurnal variations under quiet conditions on May 9–10, 2024, before the onset of the magnetic storm. This is due to the difference between seasonal illumination conditions at high and middle latitudes of the Northern Hemisphere.

2. Almost immediately after SSC in the evening on May 10, 2024 at 17:00 UT, a sharp drop in the electron density at the height of the F2-layer maximum was detected regardless of the local time at the measuring point, according to the maps of longitude-time distributions of measurements from all ionosondes. By the time the storm reached its maximum intensity on May 11, 2024 at 02:00 UT (*Dst*=–412 nT), f_oF2 had decreased to 2–3 MHz according to data from mid-latitude ionosondes in Paratunka, Irkutsk, Novosibirsk, Moscow, Kaliningrad, and Juliusruh; relative deviations df_oF2 were as large as –0.5÷–0.7. The DPS-4 ionosonde in Yakutsk worked very inconsistently after the onset of the geomagnetic storm. The Ekaterinburg ionosonde when the magnetic storm intensity was maximum showed a complete absence of data (radio signal blackout), followed by technical problems in its operation until 02:30 UT on May 12, 2024. Almost all ionosondes of the high-latitude chain (Norilsk, Salekhard, Lovozero, Sodankylä) recorded a radio signal blackout on May 10–11 (the main phase of the storm) until the evening on May 12, 2024 (the recovery phase), i.e. more than one and a half days. The radio signal blackout period according to ionosonde data from Tixie Bay was slightly shorter — until the morning of May 12, 2024.

Thus, strong effects of negative ionospheric storms were observed at high and middle latitudes during the main and recovery phases of the magnetic storm.

3. With increasing magnetic activity (under conditions of ionospheric storm development), the variability in f_oF2 in the high-latitude ionosphere is lower than at midlatitudes, even in the case of such an extremely intense magnetic storm.

4. During the analyzed magnetic storm, MIT and other ionospheric ionization troughs (ring, high-latitude, etc.), as well as particle precipitation zones (auroral oval), shifted further south of the latitude range of the ionosondes of the mid-latitude Eurasian chain (42°<GMlat<54° N).

5. Additional bursts of geomagnetic activity during the recovery phase of the storm during some periods on May 11–13, 2024 were also accompanied by significant and long-term decreases in the electron density at midlatitudes, which are comparable to those observed in the main phase of the May 10–11, 2024 superstorm (f_oF2 to 2–3 MHz and relative deviations df_oF2 to –0.5÷–0.7). These decreases were observed in ionosonde data at all longitudes of the Eastern Hemisphere — over Paratunka, Irkutsk, Novosibirsk, Moscow, Kaliningrad, and Juliusruh.

The burst of geomagnetic activity at midnight on May 12–13, 2024, again led to a blackout of ionosonde radio signals for several hours in Tixie Bay, Novosibirsk, Salekhard, Lovozero, as during the main phase of the magnetic storm.

6. The recovery of the ionospheric electron density began in the second half of the day on May 13, May 14–15 at all longitudes of mid- and high-latitude Eurasia.

7. At the final stage of the magnetic storm recovery phase from the second half of May 14 and May 15, 2024, the ionospheric storm effect changed from negative to positive. There was a period of increased electron density in the mid- and high-latitude ionosphere over Eurasia with f_oF2 exceeding the level of quiet days before the onset of the magnetic disturbance on May 9–10, 2024, the iono-

spheric aftereffect. The fact of observing this effect in the high latitude region is unusual and very interesting. Analysis of spatiotemporal variations in f_oF2 based on measurement data from the high- and mid-latitude Eurasian ionosonde chains has shown that the electron density began to increase on May 14, 2024, almost simultaneously at middle and high latitudes. At the same time, at high latitudes over Europe at night on May 14–15, 2024, the relative variations in df_oF2 were even greater (~0.4) than at midlatitudes (~0.3), compared with their values during the quiet days on May 9–10, 2024 before the onset of the magnetic storm.

8. The longitude-time distribution of [O]/[N_2] in the atmospheric gas column at thermospheric (ionospheric) heights above ~100 km for the mid-latitude region of Eurasia (54°–56° N), obtained from satellite measurements of the GUVI/TIMED UV spectrometer, explained in detail the features of the ionospheric plasma response to the extreme geomagnetic disturbance, which were revealed in the data from the mid-latitude ionosonde chain. A sharp and strong decrease in f_oF2 (~50–70 % of f_oF2 under quiet conditions) in the ionosphere of mid-latitude Eurasia began almost from the moment of the sudden commencement of the magnetic superstorm and lasted throughout the main phase and for more than two days until the evening on May 13, 2024 during the recovery phase of the magnetic storm. Such a long-lasting negative disturbance of the electron density, covering a vast territory of mid-latitude Eurasia, was caused by an extreme, catastrophic drop in [O]/[N_2] for almost three days during the superstorm.

9. It is of great scientific interest and relevance to compare the intensity of the response of the thermospheric neutral gas composition during the strongest geomagnetic events of the 21st century: the magnetic superstorm in May 2024 (*Dst*=–412 nT), analyzed in this work, and the magnetic superstorms in the fall of 2003: October 29–31 (*Dst*=–401 nT) and November 20 (*Dst*=–472 nT). The comparison was made using GUVI/TIMED measurement data on [O]/[N_2] for thermospheric heights above 100 km [https://guvitimed.jhuapl.edu/guvi]. The reaction of the neutral gas thermospheric composition to the processes developing at high latitudes of the Northern Hemisphere on May 10–15, 2024 was more global, with penetration of the thermospheric disturbance at almost all longitudes up to near-equatorial latitudes (~10° N) and with very low [O]/[N_2] ~0.1÷0.4.

During the October–November 2003 superstorms, the regions of decreased [O]/[N_2] in the Northern Hemisphere did not have global longitude coverage and were located over the longitude sector of the Atlantic Ocean and the east coast of North America on October 30–31, 2003 and over the longitude sector of the Pacific Ocean, over the territory of North America on November 20, 2003; by November 21, the region of low [O]/[N_2] shifted to the west and was situated over the eastern Pacific Ocean and over the Far East and Eastern Siberia. Over these longitude regions, the boundary of the region of decreased [O]/[N_2] dropped to ~20–30° N. At other longitudes, the boundary of low [O]/[N_2] was at midlatitudes in the range 50–60° N.

Due to such considerable differences between spatiotemporal variations in the thermospheric composition of neutral gas during the most extreme geomagnetic storms of the 21st century, we can conclude that the ionospheric response at different longitudes and latitudes of the Northern Hemisphere to such intense geomagnetic disturbances is significantly different. The magnetic superstorm in May 2024 was much more geoeffective than the superstorm in October–November 2003.

10. In view of the observed differences in the ionospheric response to extremely intense geomagnetic disturbances in three solar cycles (23, 24, and 25), we should note the role of seasonal factors in forming the ionospheric response. The ionospheric response to the May 2024 magnetic storm developed under the summer scenario, when the negative ionospheric storm effect is predominant. The same ionospheric response in the form of a negative ionospheric storm was recorded by the same ionosonde chains to the June 2015 extreme geomagnetic storm. The change in the effect of the positive ionospheric storm to the negative one (both for the superstorms in October–November 2003 and for the severest magnetic storm of solar cycle 24 in March 2015) is frequent during the equinox periods.

The research was financially supported by the Russian Science Foundation (Project No. 25-17-00187, https:// rscf.ru/en/project/25-17-00187/). The works on observations and data pre-processing were supported by the Ministry of Science and Higher Education of the Russian Federation. The results were partially obtained using the equipment of the Core Shared Research Facility “Angara” of ISTP SB RAS [http://ckp-rf.ru/catalog/ckp/3056/]. The works on observations and data pre-processing were partially carried out with the support from the Ministry of Science and Higher Education of the Russian Federation (Project FWZZ-2022-0019); under the Government assignment (State Registration Number 122011700182-1); under clause 6.2. of the plan of Roshydromet RTW "Development of Methods and Means of Ground-Based Monitoring of the Geophysical Conditions over the Arctic". The ionosonde data from Sodankylä, Průhonice, and Juliusruh were taken from the UK Solar System Data Center [https://www.ukssdc.ac.uk]. The GUVI/TIMED data used in this work was provided with support from the NASA MO&DA program. The GUVI instrument was devised and built by the Aerospace Corporation and the Johns Hopkins University. The Chief Scientist is Larry J. Paxton.

REFERENCES

Aladjev G.A., Evstafiev O.V., Mingalev V.S., et al. Interpretation of ionospheric F-region structures in the vicinity of ionization trough observed by satellite radio tomography. *Ann. Geophys.* 2001, vol. 19, pp. 25–36.

Araujo-Pradere E.A., Fuller-Rowell T.J., Codrescu M.V., Bilitza D. Characteristics of the ionospheric variability as a function of season, latitude, local time, and geomagnetic activity. *Radio Sci*. 2005, vol. 40, RS5009. DOI: 10.1029/2004RS003179.

Astafyeva E.I. Dayside ionospheric uplift during strong geomagnetic storms as detected by the CHAMP, SAC-C, TOPEX and Jason-1 satellites. *Adv. Space Res.* 2009, vol. 43, pp. 1749–1756. DOI: 10.1016/j.asr.2008.09.036.

Berger T.E., Dominique M., Lucas G., et al. The thermosphere is a drag: the 2022 Starlink incident and the threat of geomagnetic storms to low earth orbit space operations. *Space Weather*. 2023, vol. 21, iss. 3, pp. 1–15. DOI: 10.1029/2022SW003330.

Blanch E., Altadill D., Boška J., et al. November 2003 event: Effects on the Earth's ionosphere observed from ground-based ionosonde and GPS data. *Ann. Geophys.* 2005, vol. 23, iss. 9, pp. 3027–3034.

Bojilova R., Mukhtarov P., Pancheva D. Global ionospheric response during extreme geomagnetic storm in May 2024. *Remote Sensing*. 2024, iss. 21, 4046. DOI: 10.3390/rs16214046.

Buonsanto M.J. Ionospheric storms — a review. *Space Sci. Rev.* 1999, vol. 88, pp. 563–601. DOI: 10.1023/A:1005107532631.

Burešová D., Laštovička J., de Franceschi G. Manifestation of strong geomagnetic storms in the ionosphere above Europe. *Space Weather*. Springer, 2007, pp. 185–202. DOI: 10.1007/1-4020-5446-7_17.

Chernigovskaya M.A., Shpynev B.G., Yasyukevich A.S., et al. Longitudinal variations of geomagnetic and ionospheric parameters in the Northern Hemisphere during magnetic storms according to multi-instrument observations. *Adv. Space Res.* 2021, vol. 67, iss. 2, pp. 762–776. DOI: 10.1016/j.asr.2020.10.028.

Chernigovskaya M.A., Yasyukevich A.S., Khabituev D.S. Ionospheric longitudinal variability in the Northern Hemisphere during magnetic storms in March 2012 from ionosonde and GPS/GLONASS data. *Sol.-Terr. Phys*. 2023, vol. 9, iss. 4, pp. 99–110. DOI: 10.12737/stp-94202313.

Chernigovskaya M.A., Setov A.G., Ratovsky K.G., et al. Variability of ionospheric ionization over Eurasia according to data from a high-latitude ionosonde chain during extreme magnetic storms in 2015. *Sol.-Terr. Phys*. 2024a, vol. 10, iss. 2, pp. 34–47. DOI: 10.12737/stp-102202404.

Chernigovskaya M.A., Ratovsky K.G., Zherebtsov G.A., Setov A.G., Khabituev D.S., Kalishin A.S., et al. Ionospheric response over the high and middle latitude regions of Eurasia according to ionosonde data during the severe magnetic storm in March 2015. *Sol.-Terr. Phys*. 2024b, vol. 10, iss. 4, pp. 46–58. DOI: 10.12737/stp-104202406.

Chernigovskaya M.A., Ratovsky K G., Setov A.G., et al. Spatio-temporal variability of ionospheric parameters over Eurasia at middle and high latitudes during the superstorm in May 2024. *Geomagnetism and Aeronomy*. 2026, vol. 66, iss. 1, pp. 45–78. (In Russian).

Chernyshov A.A., Klimenko M.V., Nosikov I.A., et al. Effects in the upper atmosphere and ionosphere in the subauroral region during Victory Day 2024 geomagnetic storm (May 10–12, 2024). *Adv. Space Res*. 2025, vol. 76, iss. 12, pp. 7325–7350. DOI: 10.1016/j.asr.2025.02.015.

Christensen A.B., Paxton L.J., Avery S., et al. Initial observations with the Global Ultraviolet Imager (GUVI) on the NASA TIMED satellite mission. *J. Geophys. Res*. 2003, vol. 108, iss. A12, 1451. DOI: 10.1029/2003JA009918.

Danilchuk E., Yasyukevich Y., Vesnin A., et al. Impact of the May 2024 Extreme geomagnetic storm on the ionosphere and GNSS positioning. *Remote Sensing*. 2025, vol. 17, 1492. DOI: 10.3390/rs17091492.

Danilov A.D. Long-term trends of f_oF2 independent on geomagnetic activity. *Ann. Geophys*. 2003, vol. 21, no. 5, pp. 1167–1176. DOI: 10.5194/angeo-21-1167-2003.

Danilov A.D. Response of region F to geomagnetic disturbances (review). *Geliogeofizicheskie issledovaniya* [Heliogeophysical Research]. 2013, iss. 5, pp. 1–33. (In Russian).

Deminov M.G., Shubin V.N. Empirical model of the location of the main ionospheric trough. *Geomagnetism and Aeronomy*. 2018, vol. 58, no. 3, pp. 348–355. DOI: 10.1134/S0016793218030064.

Enell C.-F., Kozlovsky A., Turunen T., et al. Comparison between manual scaling and Autoscala automatic scaling applied to Sodankylä Geophysical Observatory ionograms. *Geosci. Instrum. Method. Data System*. 2016, vol. 5, pp. 53–64. DOI: 10.5194/gi-5-53-2016.

Gopalswamy N., Yashiro S., Michalek G., et al. Solar source of the largest geomagnetic storm of cycle 23. *Geophys. Res. Lett*. 2005, vol. 32, iss. 12, L12S09. DOI: 10.1029/2004GL021639.

Grandin M., Bruus E., Ledvina V.E., et al. The geomagnetic superstorm of 10 May 2024: Citizen science observations. *EGUsphere* [preprint]. 2024. DOI: 10.5194/egusphere-2024-2174.

Habarulema J.B., Katamzi Z.T., Yizengaw E., et al. Simultaneous storm time equatorward and poleward large-scale TIDs on a global scale. *Geophys. Res. Lett*. 2016, vol. 43, pp. 6678–6686. DOI: 10.1002/2016GL069740.

Hayakawa H., Ebihara Y., Mishev A., et al. The solar and geomagnetic storms in May 2024: A flash data report. *Astrophys. J.* 2025. vol. 979, 49. DOI: 10.3847/1538-4357/ad9335.

Kalishin A.S., Blagoveshchenskaya N.F., Troshichev O.A., Frank-Kamenetskii A.V. FGBU «AARI». Geophysical research in high latitudes. *Vestnik RFFI. Antarktida i Arktika: Polyarnye issledovaniya*. 2020, no. 3-4 (107-108), pp. 60–74. DOI: 10.22204/2410-4639-2020-106-107-3-4-60-78. (In Russian).

Kane R.P. Ionospheric f_oF2 anomalies during some intense geomagnetic storms. *Ann. Geophys*. 2005, vol. 23, pp. 2487–2499. DOI: 10.5194/angeo-23-2487-2005.

Karpachev A.T. The dependence of the main ionospheric trough shape on longitude, altitude, season, local time, and solar and magnetic activity. *Geomagnetism and Aeronomy*. 2003, vol. 43, no. 2, pp. 239–251.

Karpachev A. Sub-auroral, mid-latitude, and low-latitude troughs during severe geomagnetic storms. *Remote Sens*. 2021, vol. 13, no. 3, 534. DOI: 10.3390/rs13030534.2021.

Klimenko M.V., Klimenko V.V., Ratovsky K.G., et al. Numerical modeling of ionospheric effects in the middle- and low-latitude F region during geomagnetic storm sequence of 9–14 September 2005. *Radio Sci*. 2011, vol. 46, RS0D03. DOI: 10.1029/ 2010RS004590.

Klimenko M.V., Klimenko V.V., Despirak I.V., et al. Disturbances of the thermosphere-ionosphere-plasmasphere system and auroral electrojet at 30° E longitude during the St. Patrick's Day geomagnetic storm on 17–23 March 2015. *J. Atmos. Solar-Terr. Phys*. 2018, vol. 180, pp. 78–92. DOI: 10.1016/j.jastp.2017.12.017.

Krasheninnikov I., Pezzopane M., Scotto C. Application of Autoscala to ionograms recorded by the AIS-Parus ionosonde. *Computers and Geosciences*. 2010, vol. 36, pp. 628–635. DOI: 10.1016/j.cageo.2009.09.013.

Kwak Y.S., Kim J.H., Kim S., et al. Observational overview of the May 2024 G5-level geomagnetic storm: From solar eruptions to terrestrial consequences. *J. Astron. Space Sci*. 2024, vol. 41, iss. 3, pp. 171–194. DOI: 10.5140/JASS.2024.41.3.171.

Laštovička J. Monitoring and forecasting of ionospheric space weather effects of geomagnetic storms. *J. Atmos. Solar-Terr. Phys*. 2002, vol. 64, pp. 697–705. DOI: 10.1016/S1364-6826(02)00031-7.

Liou K., Newell P.T., Anderson B.J., et al. Neutral composition effects on ionospheric storms at middle and low latitudes. *J. Geophys. Res*. 2005, vol. 110, A05309. DOI: 10.1029/2004JA010840.

Loewe C.A., Prölss G.W. Classification and mean behavior of magnetic storms. *J. Geophys. Res*. 1997, vol. 102, no. A7, pp. 14,209–14,213.

MacDougall J.W., Grant I.F., Shen X. The Canadian Advanced Digital Ionosonde: Design and results. *Ionosonde Networks and Stations. WDC a for Solar-Terrestrial Physics Report UAG-104*. Boulder, 1995, pp. 21–27.

Mamrukov A.P., Khalipov V.L., Filippov L.D., et al. Geophysical information on oblique radio reflections at high latitudes and their classification. *Issledovaniya po geomagnetizmu, aehronomii i fizike Solntsa* [Research on Geomagnetism, Aeronomy and Solar Physics]. Novosibirsk, SB RAS Publ., 2000, vol. 111, pp. 14–27. (In Russian).

Matsushita S. A study of the morphology of ionospheric storms. *J. Geophys. Res*. 1959, vol. 64, iss. 3, pp. 305–321. DOI: 10.1029/JZ064i003p00305.

Mayr H.G., Volland H. Magnetic storm effects in the neutral composition. *Planet. Space Sci*. 1972, vol. 20, pp. 379–393. DOI: 10.1016/0032-0633(72)90036-0.

Mendillo M. Storms in the ionosphere: Patterns and processes for total electron content. *Rev. Geophys*. 2006, vol. 44, RG4001. DOI: 10.1029/2005RG000193.

Mikhailov A.V. Ionospheric F2-layer storms. *Física de la Tierra*. 2000, vol. 12, pp. 223–262.

Namgaladze A.A., Korenkov Yu.N., Klimenko V.V., et al. Global model of the thermosphere–ionosphere–protonosphere system. *PAGEOPH*. 1988, vol. 127, no. 2/3, pp. 219–254.

Newell P.T., Liou K., Zhang Y., et al. OVATION Prime-2013: Extension of auroral precipitation model to higher disturbance levels. *Space Weather*. 2014, vol. 12, pp. 368–379. DOI: 10.1002/2014SW001056.

Podlesnyi A.V., Brynko I.G., Kurkin V.I., et al. Multifunctional chirp ionosonde for monitoring the ionosphere. *Geliogeofizicheskie issledovaniya (Heliogeophysical Research)*. 2013, vol. 4, pp. 24–31. (In Russian).

Prölss G.W. Ionospheric F-region storms. *Handbook of atmospheric electrodynamics*. Boca Raton, CRC Press, 1995, vol. 2, ch. 8, pp. 195–248.

Prölss G.W., Werner S. Vibrationally excited nitrogen and oxygen and the origin of negative ionospheric storms. *J. Geophys. Res*. 2002, vol. 107, iss. A2, 1016. DOI: 10.1029/2001JA900126.

Polyakov V.M., Shchepkin L.A., Kazimirovsky E.S., Kokourov V.D. *Ionosfernye protsessy* [Ionospheric processes]. Novosibirsk, Nauka Publ., 1968, 535 p. (In Russian).

Ponomarchuk S.N., Zolotukhina N.A., Kurkin V.I., et al. The effects of magnetic storm on May 10–13, 2024 in the Asian region on Russia from ionospheric sounding with a continuous chirp signal. *Sol.-Terr. Phys*. 2025, vol. 11, iss. 4, pp. 14–28. DOI: 10.12737/stp-114202504.

Ratovsky K.G., Klimenko M.V., Klimenko V.V., et al. Aftereffects of geomagnetic storms: Statistical analysis and theoretical explanation. *Sol.-Terr. Phys*. 2018, vol. 4, iss. 4, pp. 26–32. DOI: 10.12737/stp-44201804.

Ratovsky K.G., Klimenko M.V., Yasyukevich Y.V., et al. Statistical analysis and interpretation of high-, mid- and low-latitude responses in regional electron content to geomagnetic storms. *Atmosphere*. 2020, vol. 11, iss. 12, p. 1308. DOI: 10.3390/atmos11121308.

Reinisch B.W., Haines D.M., Bibl K., et al. Ionospheric sounding support of over-the-horizon radar. *Radio Sci*. 1997, vol. 32, iss. 4, pp. 1681–1694. DOI: 10.1029/97RS00841.

Rishbeth H. How the thermospheric circulation affects the ionospheric F2-layer. *J. Atmos. Solar-Terr. Phys*. 1998, vol. 60, pp. 1385–1402. DOI: 10.1016/S1364-6826(98)00062-5.

Rodger A.S., Moffett R.J., Quegan S. The role of ion drift in the formation of ionisation troughs in the mid- and high-latitude ionosphere — a review. *J. Atmos. Terr. Phys*. 1992, vol. 54, pp. 1–30. DOI: 10.1016/0021-9169(92)90082-V.

Seaton M.J. A possible explanation of the drop in F-region critical densities accompanying major ionospheric storms. *J. Atmos. Terr. Phys*. 1956, vol. 8, pp. 122–124. DOI: 10.1016/0021-9169(56)90102-7.

Shpynev B.G., Zolotukhina N.A., Polekh N.M., et al. The ionosphere response to severe geomagnetic storm in March 2015 on the base of the data from Eurasian high-middle latitudes ionosonde chain. *J. Atmos. Solar-Terr. Phys*. 2018, vol. 180, pp. 93–105. DOI: 10.1016/j.jastp.2017.10.014.

Spogli L., Alberti T., Bagiacchi P., et al. The effects of the May 2024 Mother's Day superstorm over the Mediterranean sector: from data to public communication. *Ann. Geophys*. 2024, vol, 67, no. 2, PA218. DOI: 10.4401/ag-9117.

Sugiura M., Kamei T. *Equatorial Dst index 1957–1986. IAGA bull. 40*. Saint-Maur-des-Fosses: ISGI Publication Office, 1991. 14 p.

SWPC PRF 2541, 13 May 2024 – *The NOAA SWPC (Space Weather Prediction Center) PRF (Preliminary Report and Forecast) 2541* issued on 13 May 2024. ftp://ftp.swpc.noaa.gov/pub/warehouse (accessed May 30, 2025).

Themens D.R., Elvidge S., McCaffrey A., et al. The high latitude ionospheric response to the major May 2024 geomagnetic storm: A synoptic view. *Geophys. Res. Lett*. 2024, vol. 51, iss. 19, e2024GL111677. DOI: 10.1029/2024GL111677.

Troshichev O.A., Sormakov D.A. PC index as a proxy of the solar wind energy that entered into the magnetosphere: 3. Development of magnetic storms. *J. Atmos. Solar-Terr. Phys*. 2018, vol. 180, pp. 60–77. DOI: 10.1016/j.jastp.2017.10.012.

Tsurutani B., Mannucci A., Iijima B., et al. Global dayside ionospheric uplift and enhancement associated with interplanetary electric fields. *J. Geophys. Res*. 2004, vol. 109, A08302. DOI: 10.1029/2003JA010342.

Uma G., Brahmanandam P.S., Kakinami Y., et al. Ionospheric responses to two large geomagnetic storms over Japanese and Indian longitude sectors *J. Atmos. Solar-Terr. Phys*. 2012, vol. 74, pp. 94–110. DOI: 10.1016/j.jastp.2011.10.001.

Vystavnoi V.M., Makarova L.N., Shirochkov A.V., Egorova L.V. Research of the high-latitude ionosphere by vertical sounding using a modern digital ionosonde CADI. *Geliogeofizicheskie issledovaniya* [Heliogeophysical Research]. 2013, iss. 4, pp. 1–10. (In Russian).

Yasyukevich Yu.V., Vasiliev R.V., Rubtsov A.V., et al. Extreme magnetic storm of May 10–19, 2024: Coupling between neutral and charged components of the upper atmosphere and the effect on radio systems. *Doklady Earth Sciences*. 2025, vol. 520, 33. DOI: 10.1134/S1028334X24604978.

URL: https://giro.uml.edu/didbase/scaled.php (accessed October 3, 2025).

URL: https://www.sgo.fi/Data/Ionosonde/ionData.php (accessed October 3, 2025).

URL: http://guvitimed.jhuapl.edu/guvi-galleryl3on2 (accessed October 3, 2025).

URL: https://www.swpc.noaa.gov/noaa-scales-explanation (accessed October 3, 2025).

URL: https://wdc.kugi.kyoto-u.ac.jp/wdc/Sec3.html (accessed October 3, 2025).

URL: http://www.wdcb.ru/stp/geomag/geomagn_PC_ind.ru.html (accessed October 3, 2025)

URL: http://www.wdcb.ru/stp/data/solar.act/flux10.7/daily/ (accessed October 3, 2025).
URL: https://guvitimed.jhuapl.edu/guvi/ (accessed October 3, 2025).
URL: http://spidr2.ngdc.noaa.gov/spidr/ (accessed May 30, 2025).
URL: https://ssusi.jhuapl.edu/gal_edr-aur_cs (accessed May 30, 2025).
URL: http://ckp-rf.ru/ckp/3056/ (accessed October 3, 2025).
URL: https://www.ukssdc.ac.uk (accessed October 3, 2025).
URL: https://rscf.ru/project/25-17-00187/ (accessed October 3, 2025).

Original Russian version: Chernigovskaya M.A., Khabituev D.S., Setov A.G., et al., published in Solnechno-zemnaya fizika. 2026, vol. 12, no. 1, pp. 74–94. DOI: 10.12737/szf-121202609.

How to cite this article

Chernigovskaya M.A., Khabituev D.S., Setov A.G., et al. Thermospheric effects during the magnetic superstorms in May 2024 and October–November 2003 in the Northern Hemisphere and the ionospheric response to them. *Sol.-Terr. Phys.* 2026, vol. 12, iss. 1, pp. 68–86. DOI: 10.12737/stp-121202609.